Copy 150

NASA TM X-745

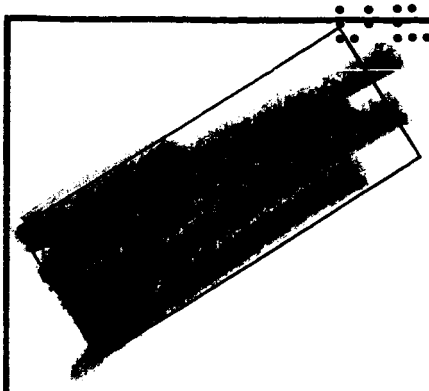

TECHNICAL MEMORANDUM

X-745

WIND-TUNNEL INVESTIGATION AT MACH NUMBERS FROM 1.60 TO 2.86 OF THE STATIC AERODYNAMIC CHARACTERISTICS OF A SUPERSONIC TRANSPORT CONFIGURATION WITH VARIABLE-SWEEP WINGS EMPLOYING A DOUBLE INBOARD PIVOT

By David S. Shaw and William P. Henderson

Langley Research Center
Langley Station, Hampton, Va.

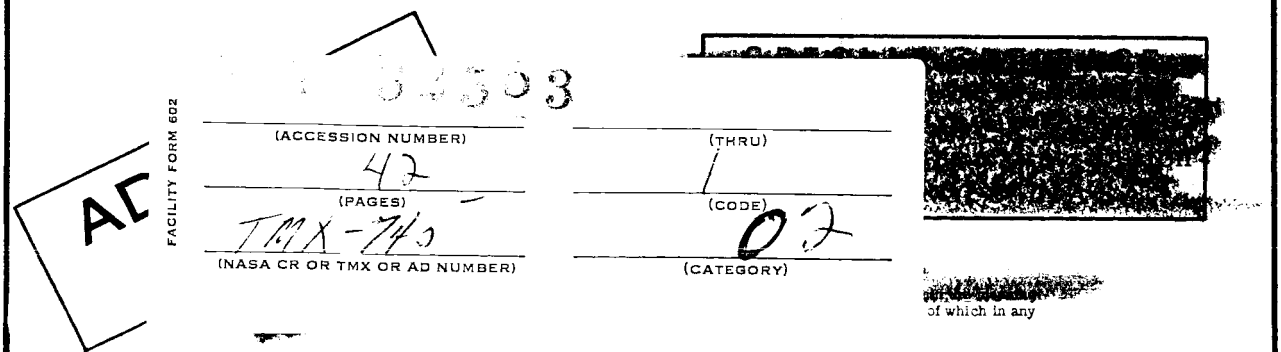

NATIONAL AERONAUTICS AND SPACE ADMINISTRATION
WASHINGTON

1H

[redacted]

NATIONAL AERONAUTICS AND SPACE ADMINISTRATION

TECHNICAL MEMORANDUM X-745

WIND-TUNNEL INVESTIGATION AT MACH NUMBERS FROM 1.60 TO 2.86 OF THE STATIC AERODYNAMIC CHARACTERISTICS OF A SUPERSONIC TRANSPORT CONFIGURATION WITH VARIABLE-SWEEP WINGS EMPLOYING A DOUBLE INBOARD PIVOT*

By David S. Shaw and William P. Henderson

ABSTRACT

The results indicate that the model is longitudinally stable at all supersonic test Mach numbers from 1.60 to 2.86 and at the test Mach number of 2.86 yields an untrimmed maximum lift-drag ratio $(L/D)_{max}$ of about 5.2. At test Reynolds number, the model with canard on yielded a trimmed L/D of about 3.9; however, with a reduction in static margin of about 0.06 mean aerodynamic chord, a trimmed L/D of about 5.1 was realized. As wing sweep was reduced from 75° to 60°, the increase in minimum drag overshadowed the reduction in drag due to lift and resulted in lower $(L/D)_{max}$. In the overall test Mach number range, the packaged engine arrangement appeared to be superior to the separate podded engines from the standpoint of aerodynamic efficiency.

*Title, Unclassified.

[redacted]

NATIONAL AERONAUTICS AND SPACE ADMINISTRATION

TECHNICAL MEMORANDUM X-745

WIND-TUNNEL INVESTIGATION AT MACH NUMBERS FROM 1.60 TO 2.86 OF THE STATIC AERODYNAMIC CHARACTERISTICS OF A SUPERSONIC TRANSPORT CONFIGURATION WITH VARIABLE-SWEEP WINGS EMPLOYING A DOUBLE INBOARD PIVOT*

By David S. Shaw and William P. Henderson

SUMMARY

An investigation was made in the Langley Unitary Plan wind tunnel to determine the supersonic aerodynamic characteristics of a double-inboard-pivot, variable-sweep, supersonic transport (SCAT 12-B) model. Tests were made at Mach numbers from 1.60 to 2.86 and at angles of attack from -6° to 11°. The test Reynolds number per foot was about 2.50×10^6. The results indicate that the model is longitudinally stable at all supersonic test Mach numbers from 1.60 to 2.86 and at the test Mach number of 2.86 yields an untrimmed maximum lift-drag ratio $(L/D)_{max}$ of about 5.2. At test Reynolds number, the model with canard on yielded a trimmed L/D of about 3.9; however, with a reduction in static margin of about 0.06 mean aerodynamic chord, a trimmed L/D of about 5.1 was realized. As wing sweep was reduced from 75° to 60°, the increase in minimum drag overshadowed the reduction in drag due to lift and resulted in lower $(L/D)_{max}$. In the overall test Mach number range, the packaged engine arrangement appeared to be superior to the separate podded engines from the standpoint of aerodynamic efficiency.

INTRODUCTION

The National Aeronautics and Space Administration is currently studying the aerodynamic characteristics of configurations which may be suitable for supersonic commercial air transport (SCAT) airplanes and is directing these studies toward cruise at Mach numbers of approximately 3. Many configuration studies have been made at Mach 3 on large bomber configurations (for example, refs. 1 and 2) and some studies have been made on transport-type configurations in this Mach number range (for example, refs. 3 to 5). These studies have been primarily directed toward thin, low-aspect-ratio wing configurations and have indicated the feasibility of designing a supersonic transport with intercontinental capability. Based

*Title, Unclassified.

on propulsive and aerodynamic efficiencies, however, indications are that these machines cannot compete favorably with present-day subsonic jet transports because of off-design operation and shorter routing necessary to realize full aircraft utilization. In order to obtain a configuration with optimum aerodynamic characteristics throughout the flight regime, some method of varying the geometry of the wing may be required. One such method of obtaining variable geometry is to have a configuration whose wing sweep angle may be varied in flight. This variation in sweep angle would provide the configuration with a high-aspect-ratio, low-sweep wing for the subsonic portions of flight, and a low-aspect-ratio, highly swept wing for the transonic and supersonic portions of flight.

One of the problems encountered with variable-sweep wings is the shift in aerodynamic center of the configuration as the wing changes sweep angle. Low-speed tests have indicated that use of a single outboard pivot location for the sweep mechanism (ref. 6) or use of a double inboard pivot with proper sizing of the forewing (ref. 7) can essentially eliminate the shift in aerodynamic center for the wing and provide a more desirable low-speed configuration. This latter type of pivot mechanism takes advantage of a retractable forewing for the unswept-wing position and an exposed forewing for the swept-wing position. In view of the promising low-speed results obtained for the configuration with the double inboard pivot, it was felt necessary to obtain supersonic aerodynamic characteristics for such a configuration.

The purpose of this paper is to present the supersonic aerodynamic characteristics obtained on a double-inboard-pivot, variable-sweep, supersonic transport configuration (designated SCAT 12-B). Tests were conducted in the Langley Unitary Plan wind tunnel at Mach numbers from 1.60 to 2.86 and at angles of attack from -6° to 11°. The test Reynolds number per foot was about 2.50×10^6.

SYMBOLS

The aerodynamic forces and moments are referred to the axes system shown in figure 1 with the origin located at the moment center shown in figure 2. The symbols used in this paper are defined as follows:

$\bar{c}$ wing mean aerodynamic chord, ft (based on $\Lambda = 75^\circ$, $\Lambda_{FW} = 79.75^\circ$)

C_D drag coefficient, $\frac{\text{Drag force}}{qS}$

$C_{D,b}$ fuselage base drag coefficient, $\frac{\text{Fuselage base drag}}{qS}$

$C_{D,c}$ chamber drag coefficient, $\frac{\text{Chamber drag}}{qS}$

$C_{D,i}$ internal drag coefficient of nacelles, $\frac{\text{Internal drag}}{qS}$

C_L	lift coefficient, $\frac{\text{Lift force}}{qS}$
C_{L_o}	lift coefficient at $\alpha = 0^\circ$
C_m	pitching-moment coefficient, $\frac{\text{Pitching moment}}{qS\bar{c}}$
C_{m_o}	pitching-moment coefficient at a lift coefficient of zero
M	free-stream Mach number
p_t	stagnation pressure, lb/sq in.
q	free-stream dynamic pressure, lb/sq ft
R	Reynolds number per foot
$R_{\bar{c}}$	Reynolds number based on $\bar{c}$ for $\Lambda = 75^\circ$, $\Lambda_{FW} = 79.75^\circ$
S	wing area, sq ft (based on $\Lambda = 75^\circ$, $\Lambda_{FW} = 79.75^\circ$)
t_t	stagnation temperature, $^\circ F$
α	angle of attack of model reference line, deg
δ_c	canard deflection angle (positive when trailing edge is down), deg
δ_h	horizontal-tail deflection angle (positive when trailing edge is down), deg
Λ	main-wing leading-edge sweep angle, deg
Λ_{FW}	leading-edge sweep angle of forewing, deg
$\frac{\partial C_D}{\partial C_L^2}$	drag-due-to-lift parameter
C_{L_α}	slope of lift curve at $C_L \approx 0$, $\partial C_L/\partial\alpha$, per deg
L/D	lift-drag ratio
$\frac{\partial C_m}{\partial C_L}$	slope of pitching-moment curve at $C_L \approx 0$

Subscripts:

max	maximum
min	minimum
trim	value of parameter at $C_m = 0$

APPARATUS AND TESTS

Tunnel

Tests were conducted in the low Mach number test section of the Langley Unitary Plan wind tunnel which is a variable-pressure, continuous-flow tunnel. The nozzle leading to the test section is of the asymmetric, sliding-block type, which permits a continuous variation in test-section Mach number from about 1.5 to 2.9.

Models

The model tested was similar to that of reference 7. The moment center used in the present report was selected on the basis of the subsonic results given in reference 7. Three-view drawings of the model are presented in figure 2 and photographs of several configurations are presented in figure 3. Area distributions of the basic model are shown in figure 4 and a list of model dimensions is presented in table I.

The wing utilized on these configurations has two pivot locations for each wing panel, one for the main wing and one for the extendible forewing. When the main-wing panel is in the fully sweptback position, the forewing is extended outward to the maximum exposed position and becomes the forward portion of the main wing; as the main-wing panel is swept forward, the forewing is retracted into the fuselage. The pivot for the main wing is located at about the 58.2-percent fuselage station and about 15.7 percent of the wing semispan when the main wing is in the 75° (basic) sweptback position. The main-wing panel has NACA 65_1A012 airfoil sections normal to the leading edge at the wing root, and NACA 65A009 airfoil sections normal to the leading edge at the wing tip.

The fuselage has an equivalent fineness ratio of 16.52.

The horizontal and vertical tails have NACA 65A002 airfoil sections in the streamwise direction. The horizontal tail could be mounted either at 0.40 inch below the model center line (low position) or at 0.10 inch above the model center line (high position), both positions having the hinge line at the 94.3-percent fuselage station.

For some of the tests, a canard consisting of a 1/16-inch flat plate with beveled leading and trailing edges was tested. The hinge line of the canard was located at the 21.1-percent fuselage station.

Two types of engine arrangements were tested: The first, a simulator to represent the inlet and ducting of a four-engine package, using the method described in reference 5, was mounted at the rear and under the fuselage (basically, this method removes the internal ducting of the engines by moving the external sides together to form a flat plate while retaining the original external wetted area and, as such, no internal drag measurements are required); the second arrangement consisted of four nacelles, two mounted on the vertical tail and two mounted from pylons under the fuselage (see fig. 2).

For the present tests, the basic configuration is considered to have: simulator on; $\Lambda = 75^\circ$; $\Lambda_{FW} = 79.75^\circ$; $\delta_h = -0.26^\circ$ (low position); canard off, and vertical tail on.

TEST CONDITIONS

Tests were performed at the following conditions:

M	t_t, °F	p_t, lb/sq in.	R/ft	$R_{\bar{c}}$
1.60	125	9.36	2.50×10^6	2.87×10^6
1.75	125	9.84	2.50	2.87
2.00	125	10.85	2.50	2.87
2.50	150	14.69	2.50	2.87
2.86	150	17.78	2.50	2.87

The dewpoint, measured at stagnation pressure, was maintained below -30° F for all tests in order to assure negligible condensation effects.

To ensure turbulent boundary-layer conditions, 1/16-inch-wide transition strips, composed of No. 120 carborundum grain (nominal size 0.006-inch diameter) were placed at the 5-percent chord of all surfaces. In addition, a ring of No. 60 carborundum grain (nominal size 0.012-inch diameter) was placed 1 inch aft of the model nose.

The test angles of attack ranged from about -6° to 11°. All tests were made at a sideslip angle of 0°.

Measurements

Aerodynamic forces and moments were measured by means of an electrical strain-gage balance housed within the model. The balance, in turn, was rigidly fastened to a sting-support system. The balance chamber pressure (used in computing chamber drag) was measured by a single static orifice located in the balance cavity. The fuselage base pressure (used in computing base drag) was measured by static orifices located at several positions around the fuselage base.

Schlieren photographs of each of the configurations tested were taken at various model attitudes and Mach numbers. Typical schlieren photographs are presented in figure 5.

Corrections

The angles of attack have been corrected for both tunnel-flow angularity and deflection of the model and sting support due to aerodynamic loads.

The drag data have been adjusted to correspond to free-stream static pressure in the balance chamber and at the fuselage base. Typical values of these corrections are shown in figure 6.

In addition to these corrections, the internal drag of the four nacelles has been estimated by considering that the nacelles are behind an oblique shock, computing the Reynolds number (based on length of nacelles), and converting the resulting skin friction into drag. The magnitude of these internal-drag corrections were:

M	$C_{D,i}$ (for four nacelles)
1.60	0.0018
1.75	.0017
2.00	.0016
2.50	.0014
2.86	.0013

ACCURACY

Based upon calibrations and repeatability of data, it is estimated that the various measured quantities are accurate within the following limits:

C_D	±0.0004
$C_{D,b}$	±0.0001
$C_{D,c}$	±0.0001
C_L	±0.0020
C_m	±0.0004
α, deg	±0.10
M	±0.015

PRESENTATION OF RESULTS

The basic results of this investigation are presented in figures 5 to 12, and some results are summarized in figures 13 to 15. An outline of the figure content is as follows:

DISCUSSION

Characteristics in Pitch, $\Lambda = 75^\circ$

The aerodynamic characteristics in pitch for the basic configuration (simulator on; $\Lambda = 75^\circ$; $\Lambda_{FW} = 79.75^\circ$; $\delta_h = -0.26^\circ$ (low position); canard off; and vertical tail on), are presented in figure 7 and summarized in figure 13. Included on these figures are results of tests with a canard surface added to the basic configuration. The basic model had a lift-curve slope near $C_L = 0$ of about 0.027

at $M = 1.60$ and the slope gradually fell off, as would be expected, to a value of about 0.023 at $M = 2.86$. Extrapolation to the design cruise speed of $M = 3.00$ indicates a value of about 0.022. The basic model was longitudinally stable and had a stability margin of about $0.23\bar{c}$ at all test Mach numbers. At $M = 2.86$, near design cruise speed, $C_{D,min}$ was about 0.0115 and the untrimmed $(L/D)_{max}$ was about 5.2. Addition of the canard, although it had no appreciable effect at negative and low positive angles of attack, slightly increased the lift at the higher test angles of attack (see fig. 7(a)) as would be expected. In addition, the canard reduced the stability margin to about $0.10\bar{c}$ at $M = 1.60$ and to about $0.13\bar{c}$ at $M = 2.86$. It is interesting to note that the canard had only a slightly adverse effect on $C_{D,min}$ (less than 0.0006 regardless of test Mach number) and the effects on $(L/D)_{max}$ were also small.

The results of tests of horizontal-tail deflection for the basic model and for the model with a canard are presented in figure 8. Negative horizontal-tail deflection leads to a decrease in C_{L_o} with no change in C_{L_α}, an increase in C_{m_o} with no change in $\partial C_m/\partial C_L$, an increase in $C_{D,min}$, and a decrease in $(L/D)_{max}$. In all of these instances, the incremental changes due to δ_h were the same, at a given Mach number, regardless of whether the canard was off or on. Because of the decrease in stability level for the model with the canard on, however, a given deflection of the horizontal tail trims the model at about twice the lift coefficient as that for the basic model with the canard off. (For example, at $M = 2.86$ for $\delta_h = -4.55^\circ$, $C_{L,trim}$ is approximately 0.033 for canard off whereas $C_{L,trim}$ is approximately 0.064 for canard on.)

The results of tests of canard deflection are presented in figure 9 and show that the canard has about the same efficiency as the horizontal tail in trimming the model. For example, at $M = 2.86$, the canard with $\delta_c = 6^\circ$ has a trim point at a C_L of approximately 0.06 with an $(L/D)_{max}$ penalty of about 0.20 and almost identical values are obtained for $\delta_h = -4.55^\circ$ as seen in figures 8(b) and 8(d). The larger canard deflection would be expected to give the same values (if there are no interference effects) since, by using the quarter chord of the mean aerodynamic chord of the exposed areas, the tail volume of the canard is only about two-thirds the tail volume of the horizontal tail.

Figure 14 shows the effect of change in static margin on $C_{L,trim}$ and $(L/D)_{trim}$ at $M = 2.86$. This figure incorporates the basic control data of figures 8 and 9 in combination with assumed changes in location of the moment center. (It should be remembered that the stability margin is $0.23\bar{c}$ for canard off and $0.13\bar{c}$ for canard on for the present moment center shown in fig. 2.) The data for δ_c = off, $\delta_h = -0.26^\circ$, and $\delta_c = 0^\circ$, $\delta_h = -0.26^\circ$ have not been presented in figure 14 since figures 8 and 9 show that for these conditions the model has negative C_{m_o}. Figure 14 shows that approximately equal maximum values of $(L/D)_{trim}$ may be reached by using either the canard or horizontal tail and that the test canard and horizontal tail are equally effective in producing trimmed L/D,

provided that the static margin can be reduced by $0.12\bar{c}$ to about $0.11\bar{c}$ for canard off or reduced by $0.06\bar{c}$ to about $0.07\bar{c}$ for canard on. These reductions yield a trimmed lift-drag ratio of about 5.1. It is difficult to ascertain the amount that the static margin may be changed since one may also change the static margin by varying the wing sweep. (See figs. 11 and 15.) If no change of static margin is allowable, the better trim device for the present moment center is the canard which yields a trimmed L/D of about 3.9 at the test Reynolds number.

In order to determine the effect of vertical position of the aft horizontal tail on the aerodynamic characteristics in pitch, the tail was raised 0.50 inch from its original position to 0.10 inch above the reference line. For both positions, the hinge line was kept at the same fuselage station. Also, for this portion of the tests, the simulator was removed from the model for both tail positions. The results of these tests are presented in figure 10 and show no significant difference for any of the longitudinal parameters.

Effect of Wing Sweep Angle

The effects of changing wing sweep angle from 75° to 60° on the aerodynamic characteristics in pitch for the model with canard on at 0° are presented in figure 11 and summarized in figure 15. As previously mentioned, all of these data have been computed on the basis of the geometric dimensions of the configuration with the wing at $\Lambda = 75^\circ$. These data show that, at the lower end of the test Mach number range where the wing leading edge is subsonic, the lower the sweep angle (the higher the aspect ratio), the higher the lift-curve slope. As the Mach number is increased and the wing approaches or exceeds a sonic leading-edge condition, the effect of aspect ratio tends to disappear. For example, at $M = 1.60$, C_{L_α} for the model with $\Lambda = 60^\circ$ is about 50 percent larger than that of the model with $\Lambda = 75^\circ$, whereas at $M = 2.86$, the differences in C_{L_α} for these two model configurations are barely noticeable.

The effects of wing sweep on the drag and lift-drag characteristics of the model are also pronounced. At the lower test Mach number, there is little or no difference in $C_{D,min}$ for the configurations with $\Lambda = 75^\circ$ or 70° and even at the higher test Mach numbers these differences in $C_{D,min}$ are small. Reducing the sweep to 60°, on the other hand, leads to sizable increases in $C_{D,min}$ at all of the test Mach numbers. Since at the lower Mach numbers all three sweep angles lead to subsonic leading-edge wings, and at $M = 2.86$, the two higher swept wings have subsonic leading edge and the $\Lambda = 60^\circ$ wing has essentially a sonic leading edge, it appears, in view of the relatively constant difference in $C_{D,min}$ for these models, that the sweep effects on $C_{D,min}$ are secondary and the change in streamwise thickness ratio with sweep angle is the primary cause for the much higher $C_{D,min}$ of the model with the $\Lambda = 60^\circ$ wing.

Figure 15, which shows a summary of the aerodynamic characteristics with sweep as a variable, shows that the lower the sweep angle of the wing leading edge, the lower the drag due to lift. This trend agrees with subsonic theory

which shows that an increase in aspect ratio results in lower drag due to lift. At the lower test Mach numbers where all three wing sweeps have subsonic leading edges, the higher aspect ratio wing with $\Lambda = 60^\circ$ has significantly lower drag-due-to-lift values. At the higher test Mach numbers, for example. at $M = 2.86$, the drag due to lift for the three model wing conditions approach each other although the $\Lambda = 60^\circ$ wing still has slightly better drag-due-to-lift characteristics. Supersonic wing theory indicates that, for a flat wing (no twist or camber) with no leading-edge suction, once the wing leading edge becomes sonic there is little or no effect of aspect ratio on drag due to lift; and therefore it should be expected that the drag-due-to-lift curves, for the three wing-sweep configurations of this test, would converge at the higher test Mach numbers.

Since the effects of wing thickness are not isolated for the current tests, the trade-off in minimum drag and drag due to lift in order to obtain the optimum L/D is not readily apparent. However, as wing sweep was reduced from 75° to 60°, the increase in minimum drag overshadowed the reduced drag due to lift and resulted in lower $(L/D)_{max}$. Calculations to determine the drag penalty involved by the difference in thickness between the $\Lambda = 75^\circ$ wing and the $\Lambda = 60^\circ$ wing indicate that appreciable gains in lift-drag ratio may be obtained by incorporating streamwise wing section thicknesses on the $\Lambda = 60^\circ$ wing that are comparable with those on the $\Lambda = 75^\circ$ wing. It should be emphasized that these effects are only applicable in the case of a flat wing. Theory (for example, ref. 8) indicates that twist and camber, if properly applied to a subsonic leading-edge wing in a supersonic stream, can lead to sizable gains in L/D.

Engine Arrangements

A comparison of the basic configuration with and without the simulated packaged engine arrangement and also with four nacelles is presented in figure 12. Removing the simulator has little effect on the lift or pitch characteristics of the model, but $C_{D,min}$ is materially reduced and $(L/D)_{max}$ is significantly increased. Adding the nacelles to the configuration slightly increased the lift-curve slope and significantly increases $C_{D,min}$. At the lower test Mach numbers, the configuration with the nacelles has an appreciably lower $(L/D)_{max}$, but at the highest test Mach number, $M = 2.86$, the $(L/D)_{max}$ for the nacelle configuration approaches that for the configuration with the simulated packaged engine arrangement. From an efficiency standpoint in the overall Mach number range of these tests, it appears that the packaged arrangement of engines will be superior to the separate podded engine arrangement. In addition, it is believed that improvements in the packaged arrangement of engines may be obtained at the higher test Mach numbers by use of a more nearly optimum diverter arrangement.

CONCLUSIONS

Results of an investigation to determine the supersonic aerodynamic characteristics of a double-inboard-pivot, variable-sweep, supersonic commercial air transport (SCAT 12-B) model indicate the following conclusions:

1. The basic model is longitudinally stable at all supersonic test Mach numbers from 1.60 to 2.86 and at the test Mach number of 2.86 yields an untrimmed maximum lift-drag ratio $(L/D)_{max}$ of about 5.2.

2. At test Reynolds number, the model with canard on yielded a trimmed L/D of about 3.9; however, with a reduction in static margin of about 0.06 mean aerodynamic chord, a trimmed L/D of about 5.1 would be realized.

3. As wing sweep was reduced from 75° to 60°, the increase in minimum drag overshadowed the reduced drag due to lift and resulted in lower $(L/D)_{max}$.

4. In the overall test Mach number range, the packaged engine arrangement appeared to be superior to the separate podded engines from the standpoint of aerodynamic efficiency.

Langley Research Center,
National Aeronautics and Space Administration,
Langley Station, Hampton, Va., September 18, 1962.

REFERENCES

1. Kelly, Thomas C., Carmel, Melvin M., and Gregory, Donald T.: An Exploratory Investigation at Mach Numbers of 2.50 and 2.87 of a Canard Bomber-Type Configuration Designed for Supersonic Cruise Flight. NACA RM L58B28, 1958.

2. Gregory, Donald T., and Carraway, Ausley B.: Investigation of the Effects of Engine Arrangement on Stability and Performance Characteristics of a Canard-Type Aircraft Configuration Near A Mach Number of 3 Including Effects of Canard Plan Form. NASA TM X-217, 1960.

3. Carraway, Ausley B., Gregory, Donald T., and Carmel, Melvin M.: An Exploratory Investigation of a Transport Configuration Designed for Supersonic Cruise Flight Near a Mach Number of 3. NASA TM X-216, 1960.

4. Morris, Owen G., Carmel, Melvin M., and Carraway, Ausley B.: An Investigation at Mach Numbers From 0.20 to 4.63 of the Aerodynamic Performance, Static Stability, and Trimming Characteristics of a Canard Configuration Designed for Efficient Supersonic Cruise Flight. NASA TM X-617, 1961.

5. Carraway, Ausley B., Morris, Owen G., and Carmel, Melvin M.: Aerodynamic Characteristics at Mach Numbers From 0.20 to 4.63 of a Canard-Type Supersonic Commercial Air Transport Configuration. NASA TM X-628, 1962.

6. Alford, William J., Jr., and Henderson, William P.: An Exploratory Investigation of the Low-Speed Aerodynamic Characteristics of Variable-Wing-Sweep Airplane Configurations. NASA TM X-142, 1959.

7. Henderson, William P.: Low-Speed Longitudinal Stability Characteristics of a Supersonic Transport Configuration With Variable-Sweep Wings Employing a Double Inboard Pivot. NASA TM X-744, 1962.

8. Brown, Clinton E., and McLean, Francis E.: The Problem of Obtaining High Lift-Drag Ratios at Supersonic Speeds. Jour. of Aero/Space Sci., vol. 26, no. 5, May 1959, pp. 298-302.

TABLE I.- MODEL COMPONENTS

Fuselage:	
Length, in.	41.64
Maximum width, in.	2.65
Maximum height, in.	2.30
Fineness ratio	16.52
Wing:	
With $\Lambda = 75^{\circ}$	
Forewing sweep angle, deg	79.75
Main-wing trailing-edge sweep angle, deg	65.35
Area (includes forewing), sq ft	1.285
Span, in.	16.528
Mean aerodynamic chord, in.	13.789
Aspect ratio (includes forewing)	1.476
With $\Lambda = 70^{\circ}$	
Forewing sweep angle, deg	80.25
Main-wing trailing-edge sweep angle, deg	60.35
Area (includes forewing), sq ft	1.234
Span, in.	19.040
Mean aerodynamic chord, in.	11.881
Aspect ratio (includes forewing)	2.039
With $\Lambda = 60^{\circ}$	
Forewing sweep angle, deg	84.00
Main-wing trailing-edge sweep angle, deg	50.35
Area (includes forewing), sq ft	1.151
Span, in.	23.780
Mean aerodynamic chord, in.	9.281
Aspect ratio (includes forewing)	3.413
Canard:	
Leading-edge sweep angle, deg	60.00
Trailing-edge sweep angle, deg	0
Tip chord, in.	0.400
Root chord, in.	5.600
Root chord (exposed), in.	3.890
Span, in.	6.000
Area (total), sq ft	0.125
Area (exposed), sq ft	0.0596
Aspect ratio (total)	2.00
Airfoil section	1/16-inch flat plate with beveled leading and trailing edges
Horizontal tail:	
Leading-edge sweep angle, deg	60.00
Trailing-edge sweep angle, deg	37.50
Tip chord, in.	2.208
Root chord, in.	6.308
Root chord (exposed), in.	5.300
Area (total), sq ft	0.252
Area (exposed), sq ft	0.1642
Span, in.	8.516
Aspect ratio (total)	2.00
Airfoil section (in streamwise direction)	NACA 65A002
Vertical tail:	
Leading-edge sweep angle, deg	60.00
Trailing-edge sweep angle, deg	37.50
Tip chord, in.	2.208
Root chord (exposed), in.	6.308
Span, in.	4.587
Airfoil section (in streamwise direction)	NACA 65A002

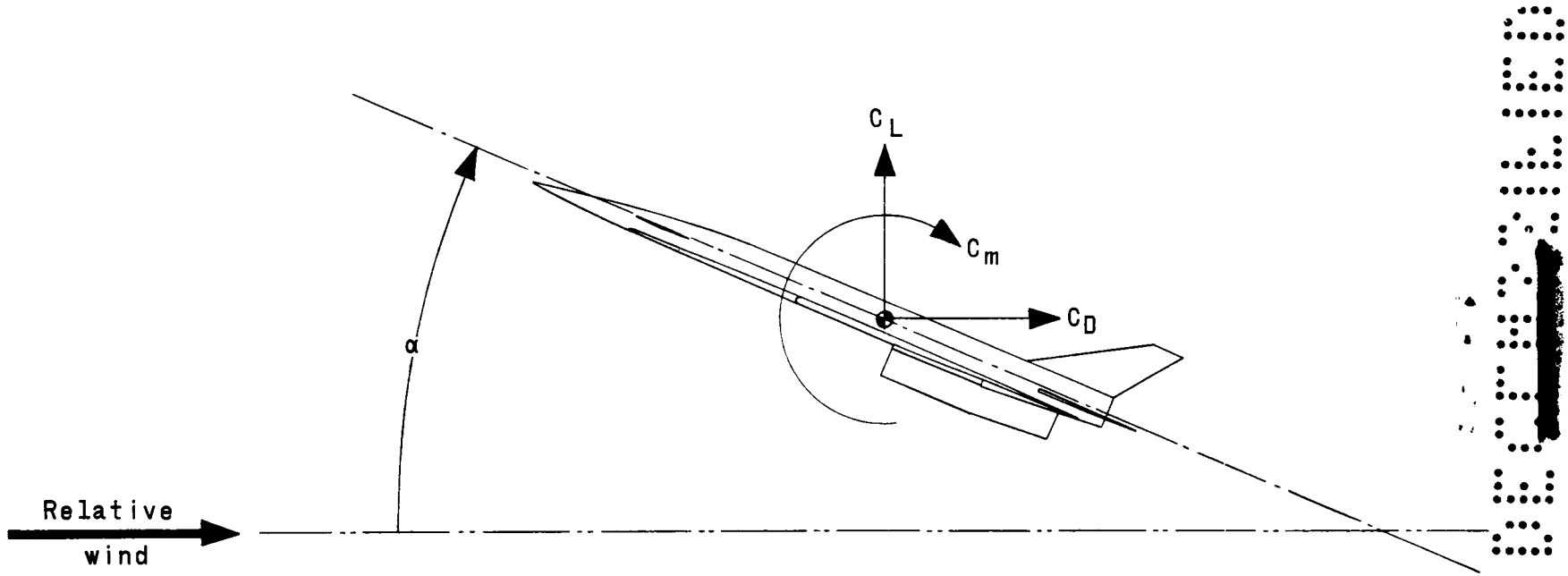

Figure 1.- Axes systems. (Arrows indicate positive directions.)

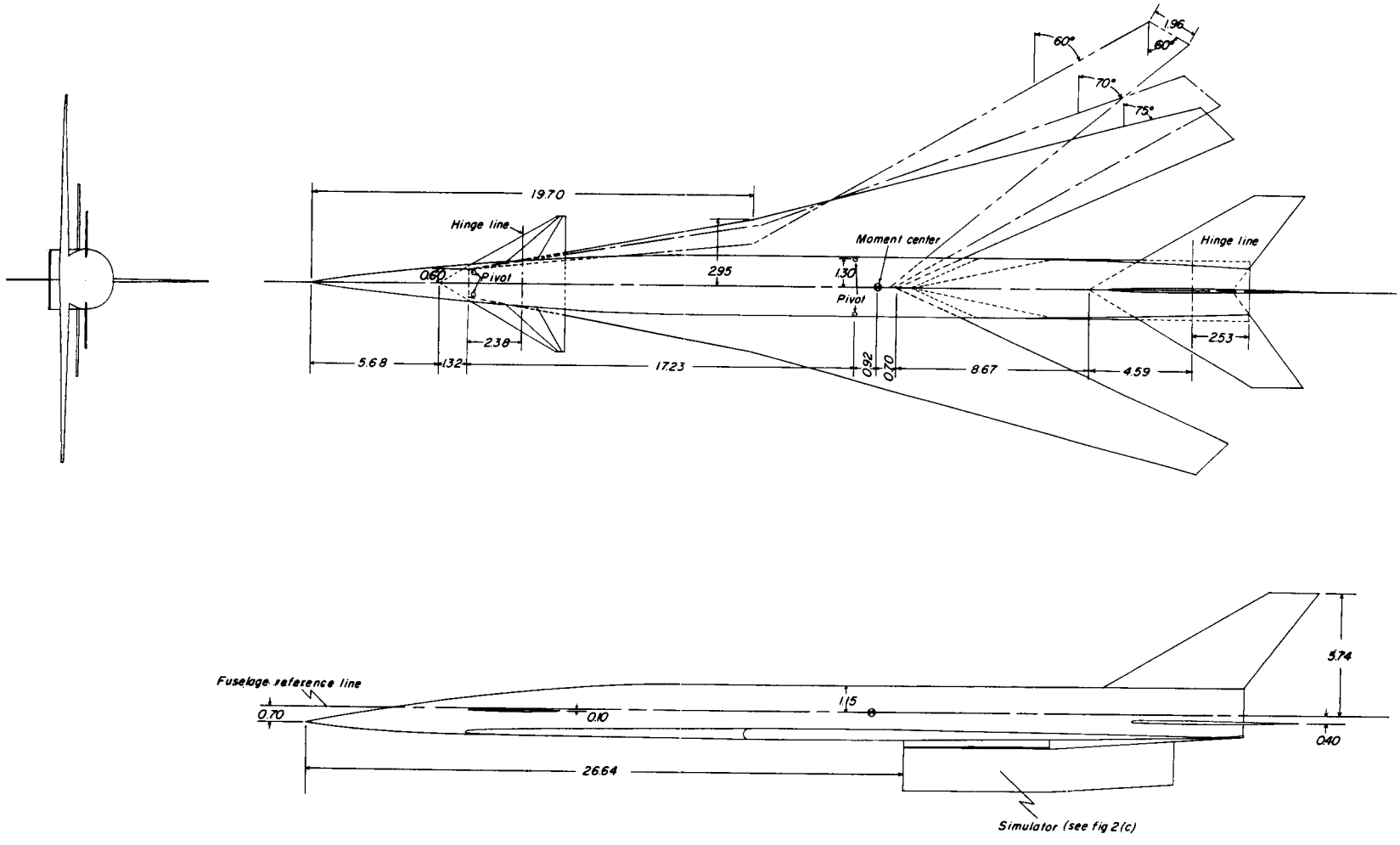

(a) Simulator on.

Figure 2.- Drawings and dimensions of models. All linear dimensions are in inches.

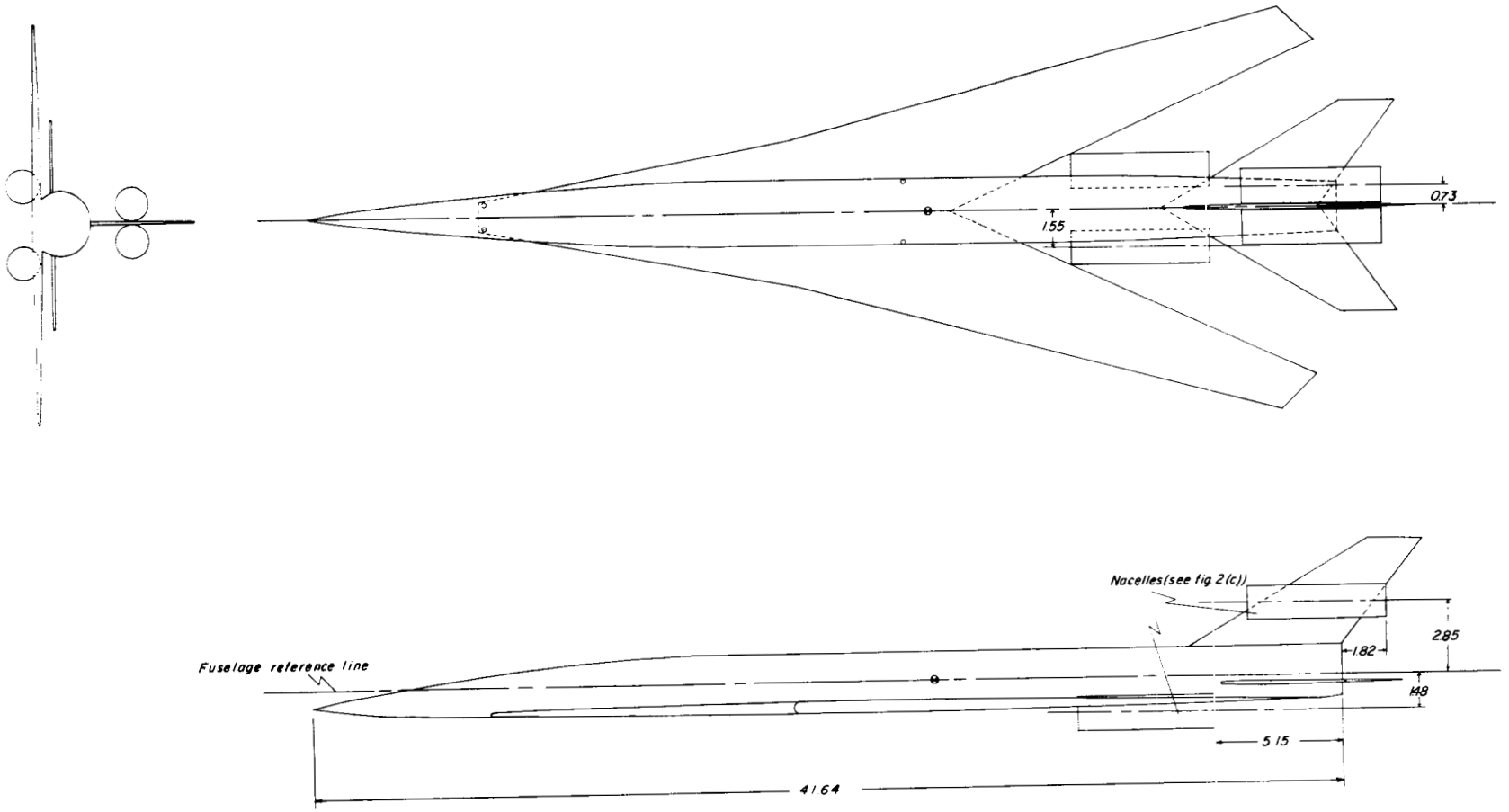

(b) Four nacelles on.

Figure 2.- Continued.

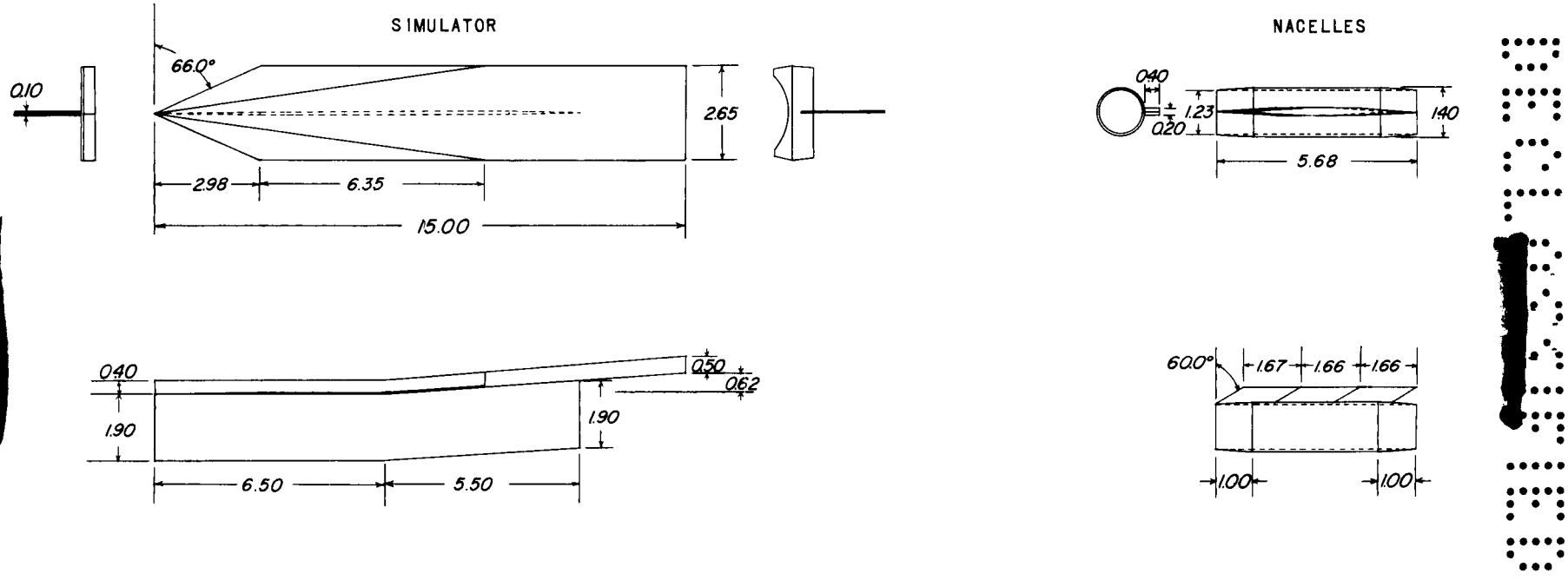

(c) Details of simulator and nacelles.

Figure 2.- Concluded.

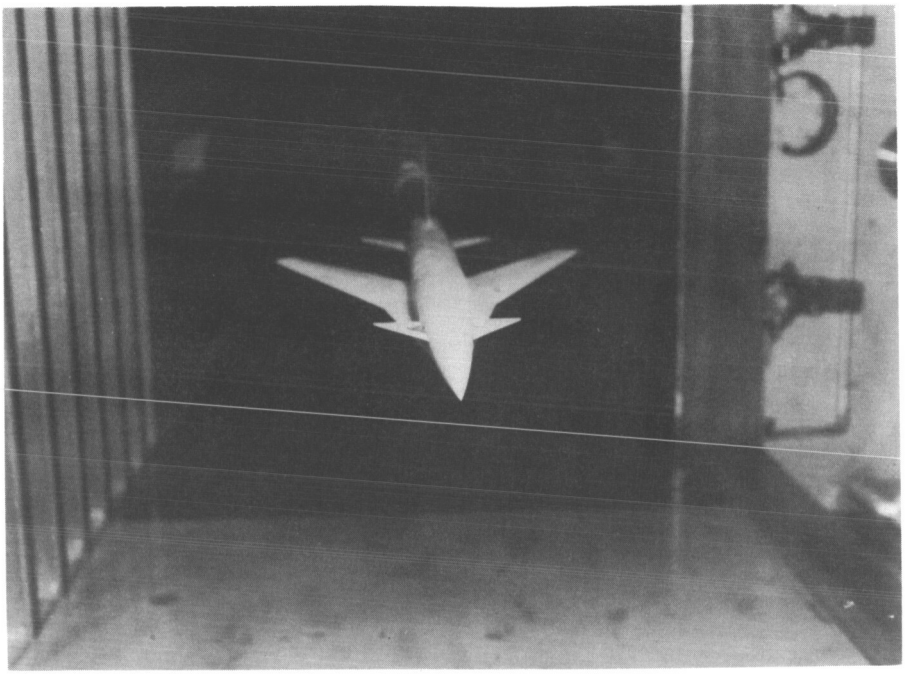

L-61-6857

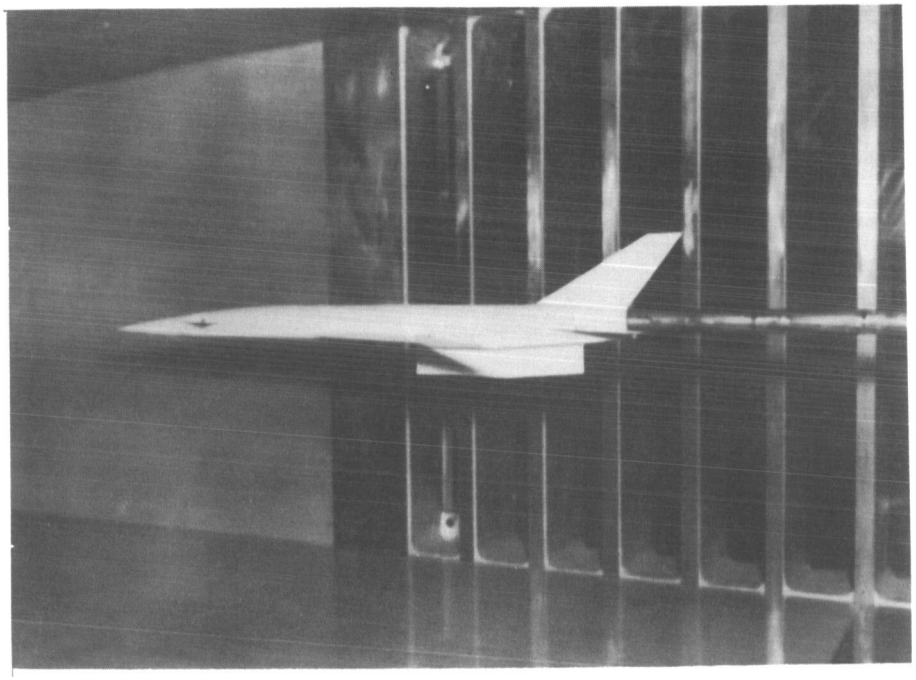

L-61-6860

(a) Simulator on; $\Lambda = 75^{\circ}$; $\Lambda_{FW} = 79.75^{\circ}$; vertical tail on; $\delta_h = -0.26^{\circ}$ (low position); $\delta_c = 0^{\circ}$.

Figure 3.- Models in test section.

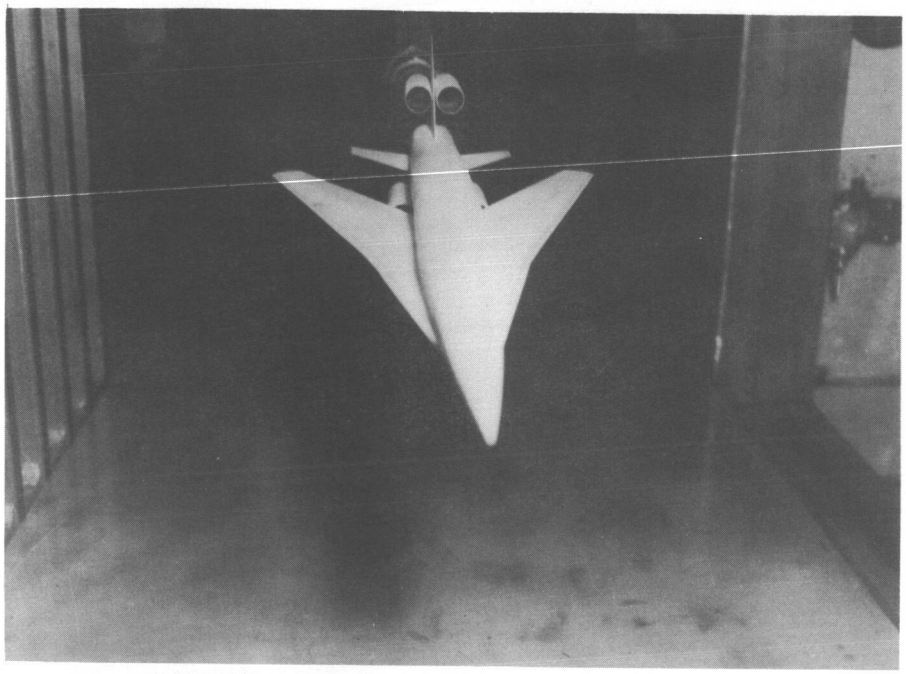

L-61-6863

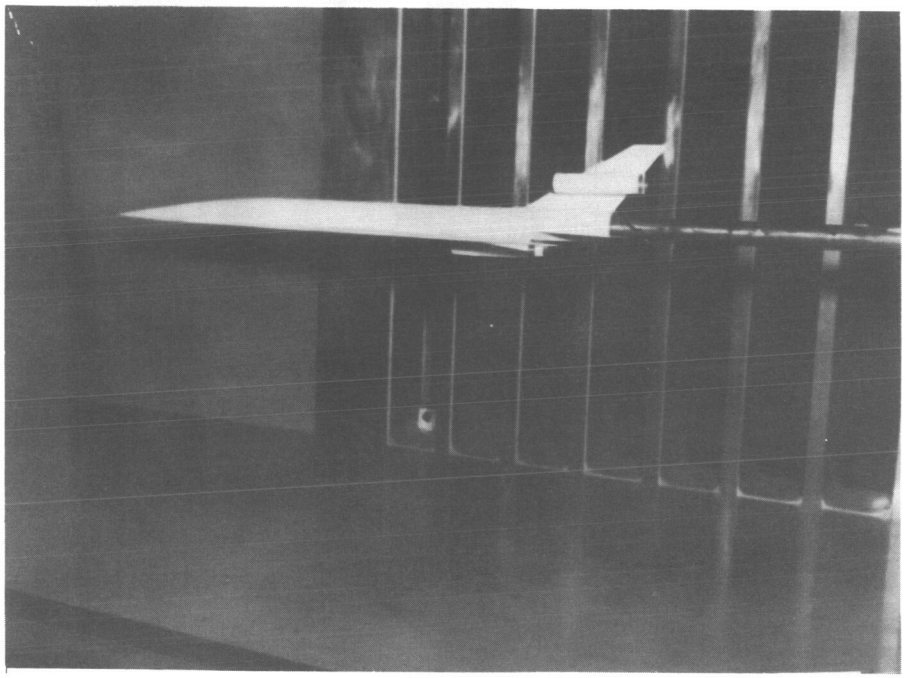

L-61-6862

(b) Nacelles on; $\Lambda = 75^{\circ}$; $\Lambda_{FW} = 79.75^{\circ}$; vertical tail on; $\delta_h = -0.26^{\circ}$ (low position); δ_c = off.

Figure 3.- Concluded.

Model component	Wetted area / Wing area
Fuselage	1.417
Wing	1.509
Horizontal tail	0.245
Vertical tail	0.196
Canard	0.093
Simulator	0.569

Total $\frac{\text{Wetted area}}{\text{Wing area}}$ =4.029

$\frac{\text{Volume}^{2/3}}{\text{Wing area}}$ =0.197

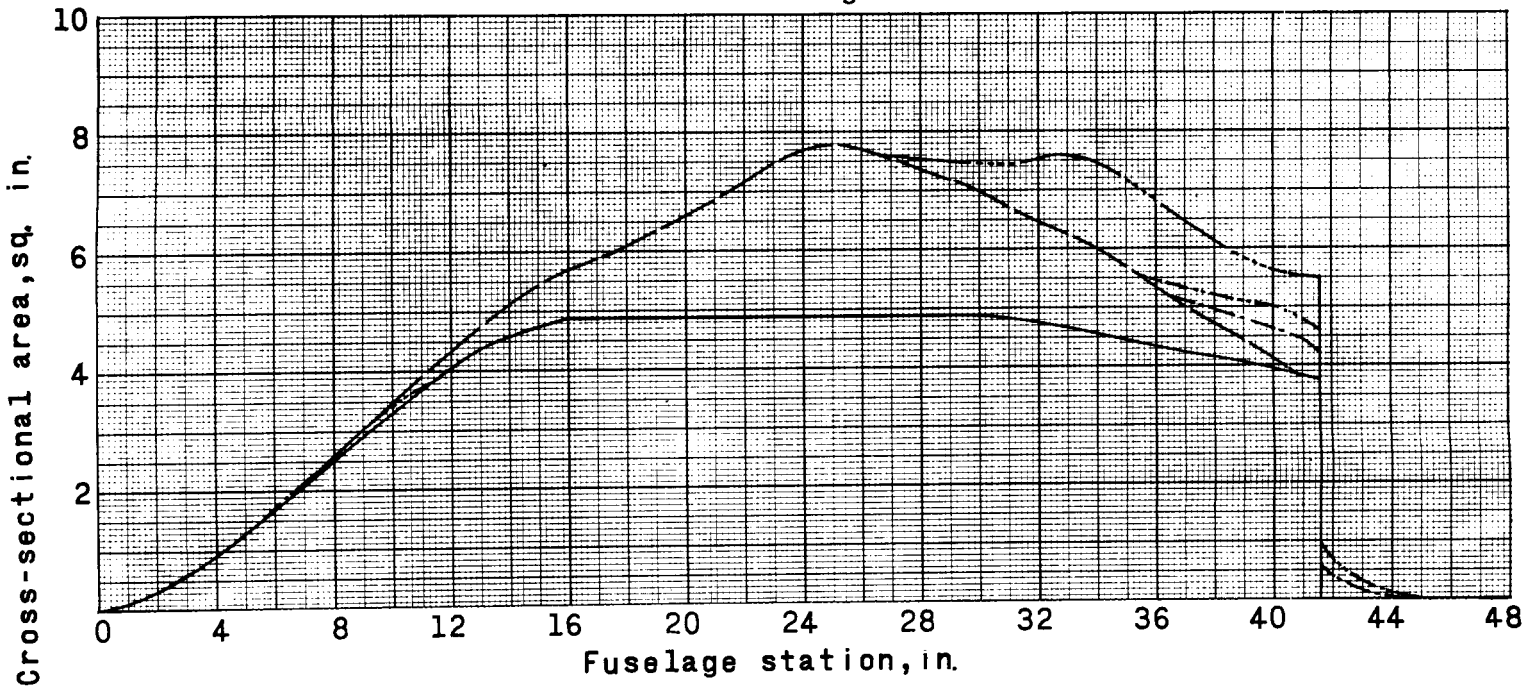

Figure 4.- Cross-sectional-area distribution and wetted areas of the basic configuration with canard on. Simulator on; $\Lambda = 75^{\circ}$; $\Lambda_{FW} = 79.75^{\circ}$; vertical tail on; horizontal tail on; canard on.

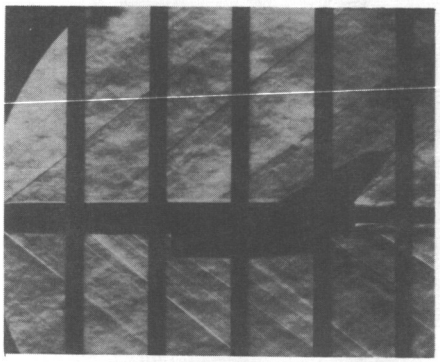

M=1.60;α=0.4°

M=1.75;α=0.4°

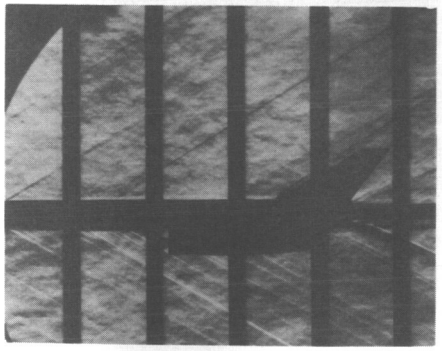

M=2.00;α=1.1°

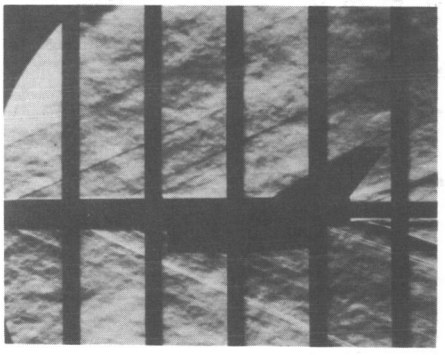

M=2.50;α=0.8°

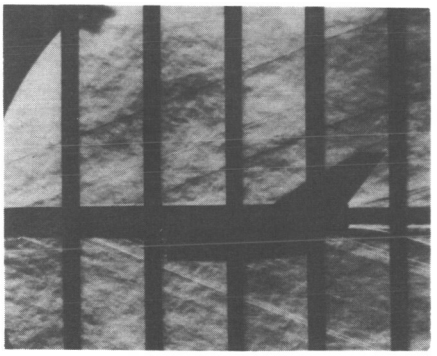

M=2.86;α=-0.5°

L-62-7015

(a) Simulator on; $\Lambda = 60^{\circ}$; vertical tail on; $\delta_h = -0.26^{\circ}$ (low position); $\delta_c = 0^{\circ}$.

Figure 5.- Typical schlieren photographs.

M=1.60;α=0.4°

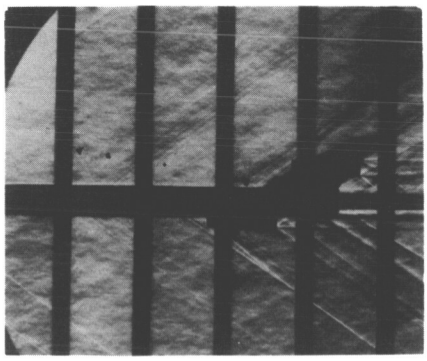

M=1.75;α=0.4°

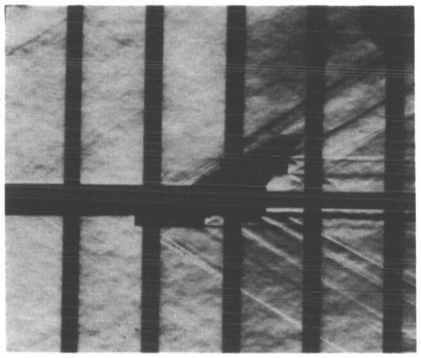

M=2.00;α=1.1°

M=2.50;α=0.8°

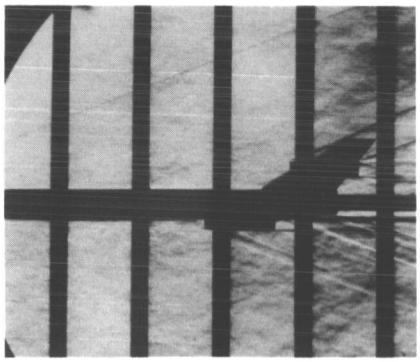

M=2.86;α=-0.5°

L-62-7016

(b) Nacelles on; $\Lambda = 75^{\circ}$; $\Lambda_{FW} = 79.75^{\circ}$; vertical tail on; $\delta_h = -0.26^{\circ}$ (low position); canard off.

Figure 5.- Concluded.

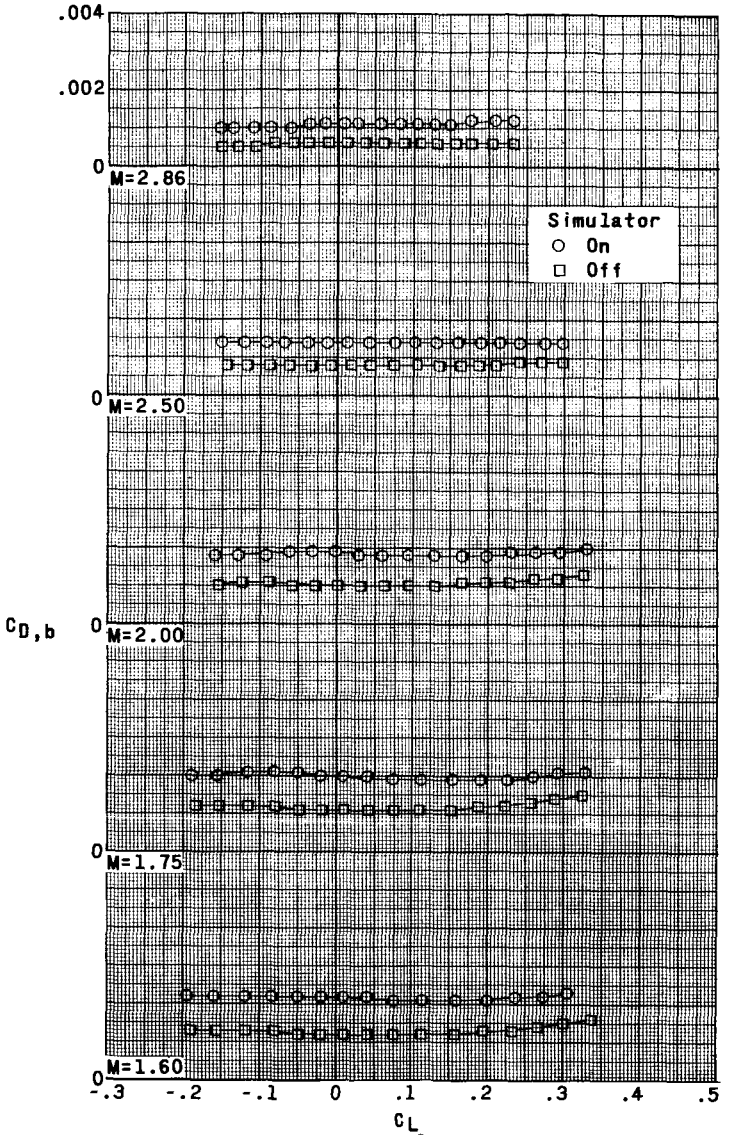

(a) Base-drag corrections.

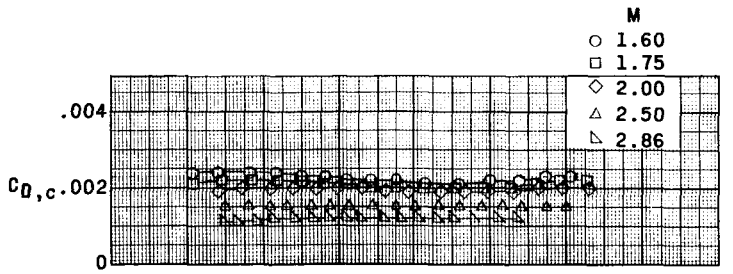

(b) Chamber-drag corrections.

Figure 6.- Typical base- and chamber-drag corrections.

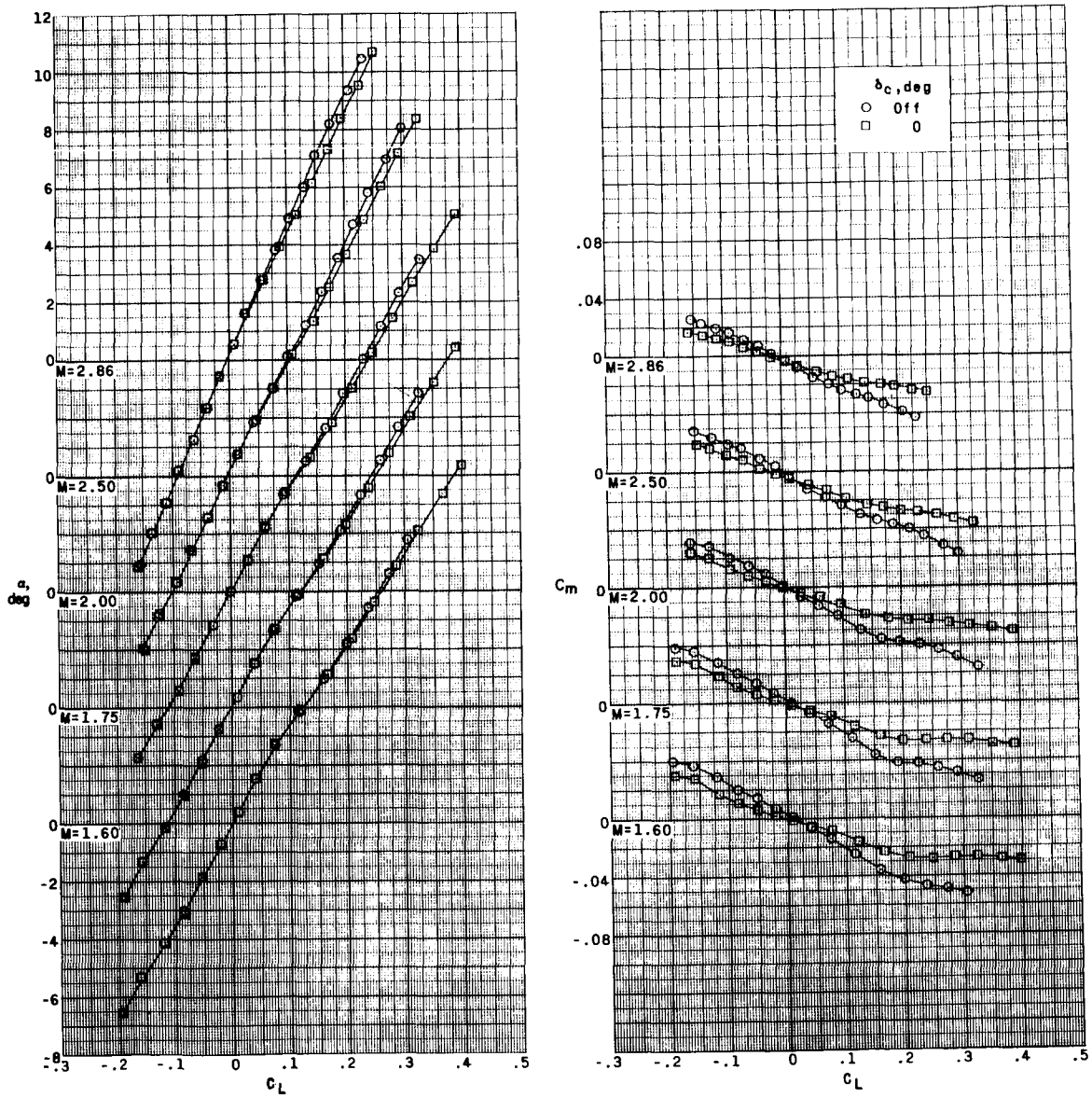

(a) Variation of α and C_m with C_L.

Figure 7.- Aerodynamic characteristics in pitch for the basic configuration both with and without a canard. Simulator on; $\Lambda = 75^\circ$; $\Lambda_{FW} = 79.75^\circ$; vertical tail on; $\delta_h = -0.26^\circ$ (low position).

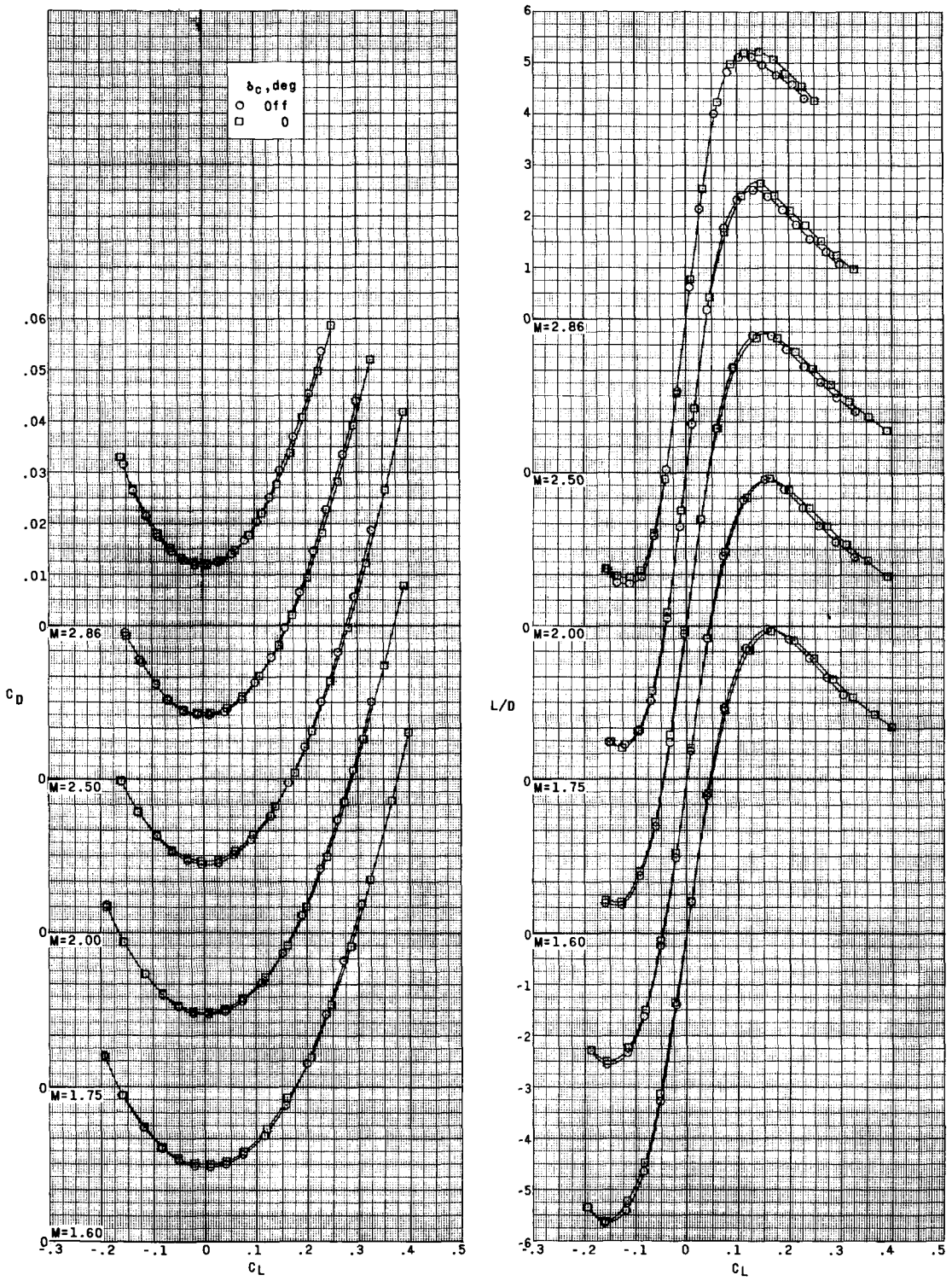

(b) Variation of C_D and L/D with C_L.

Figure 7.- Concluded.

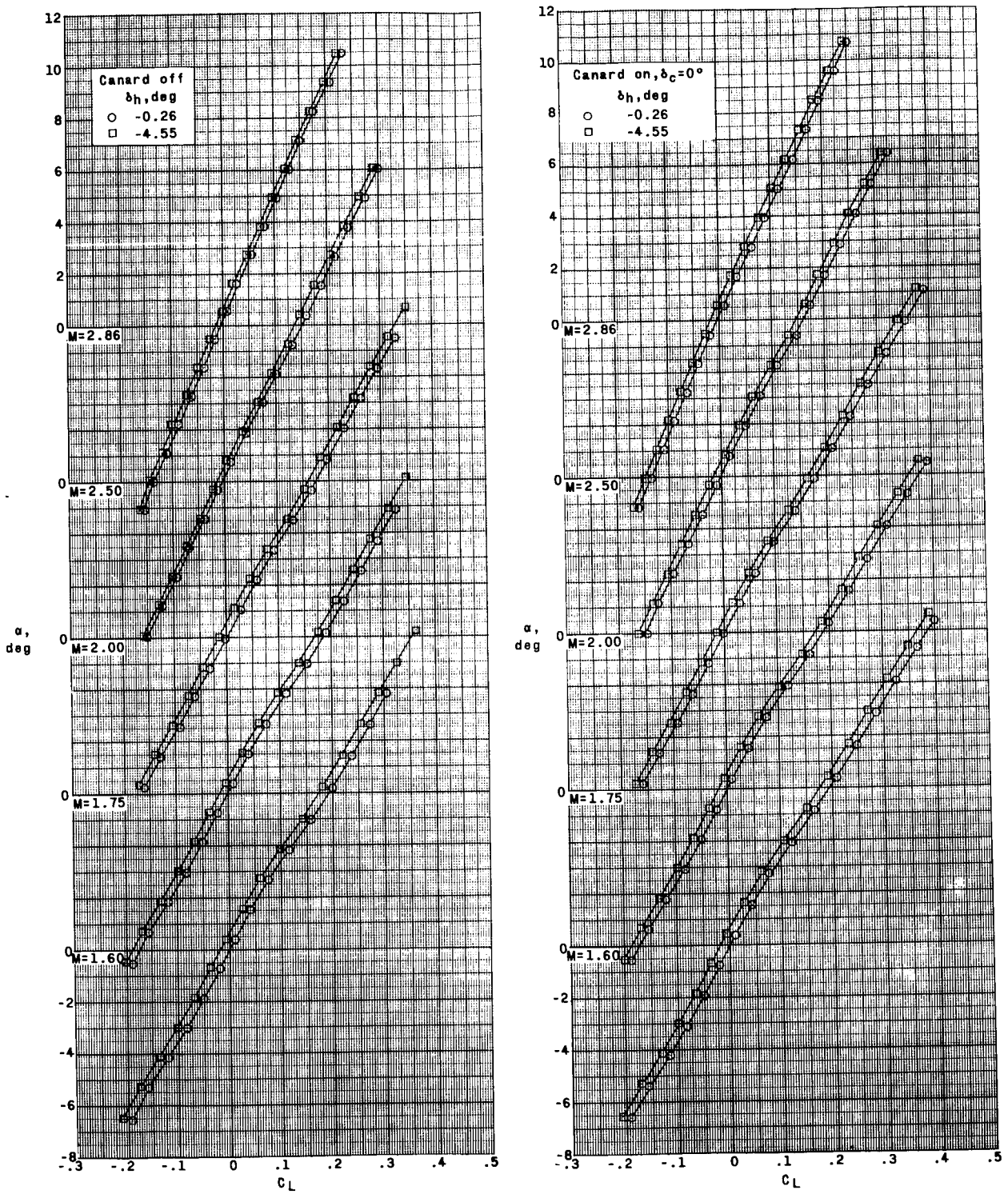

(a) Variation of α with C_L.

Figure 8.- Effect of horizontal-tail deflection on aerodynamic characteristics. Simulator on; $\Lambda = 75^\circ$; $\Lambda_{FW} = 79.75^\circ$; vertical tail on.

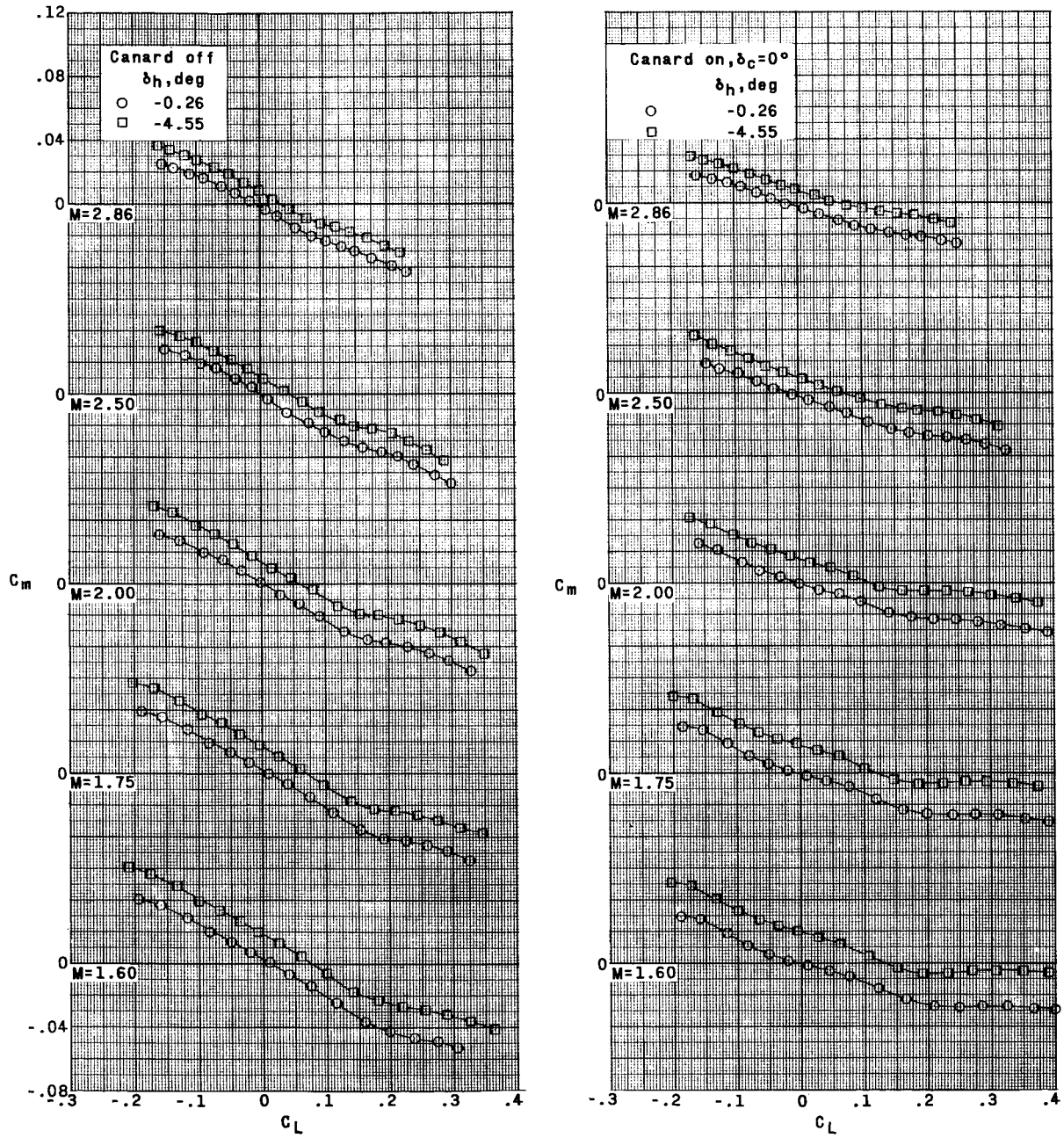

(b) Variation of C_m with C_L.

Figure 8.- Continued.

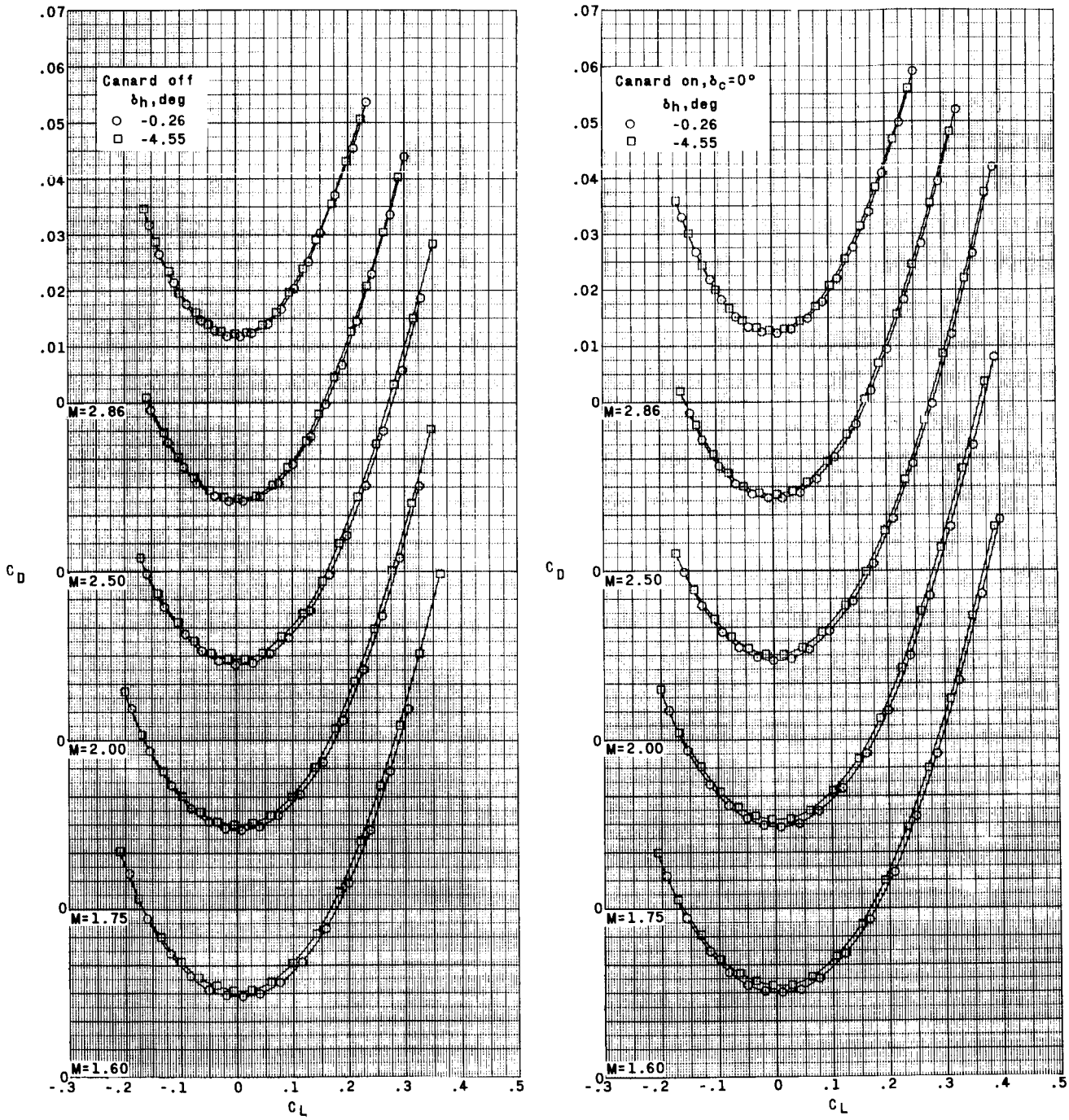

(c) Variation of C_D with C_L.

Figure 8.- Continued.

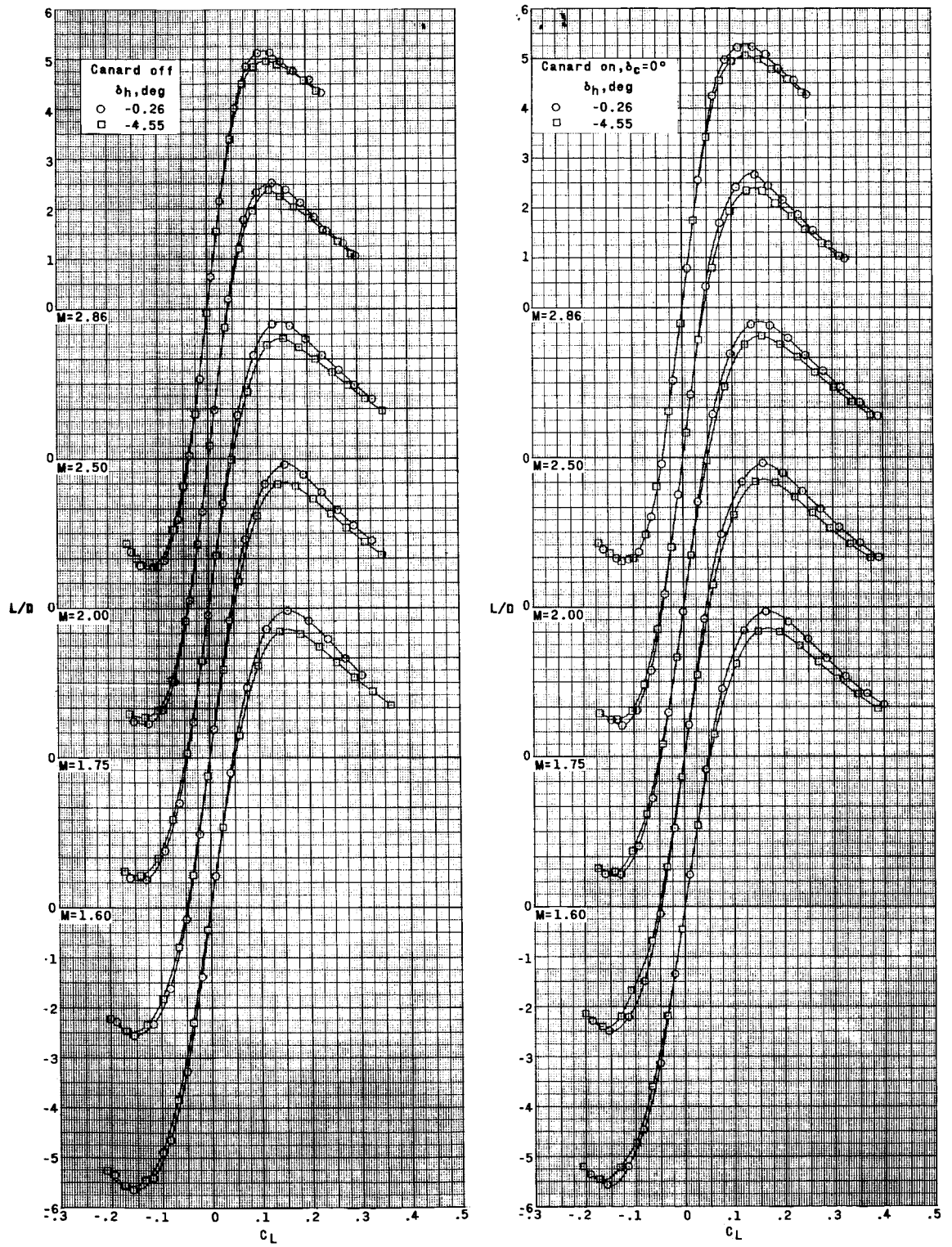

(d) Variation of L/D with C_L.

Figure 8.- Concluded.

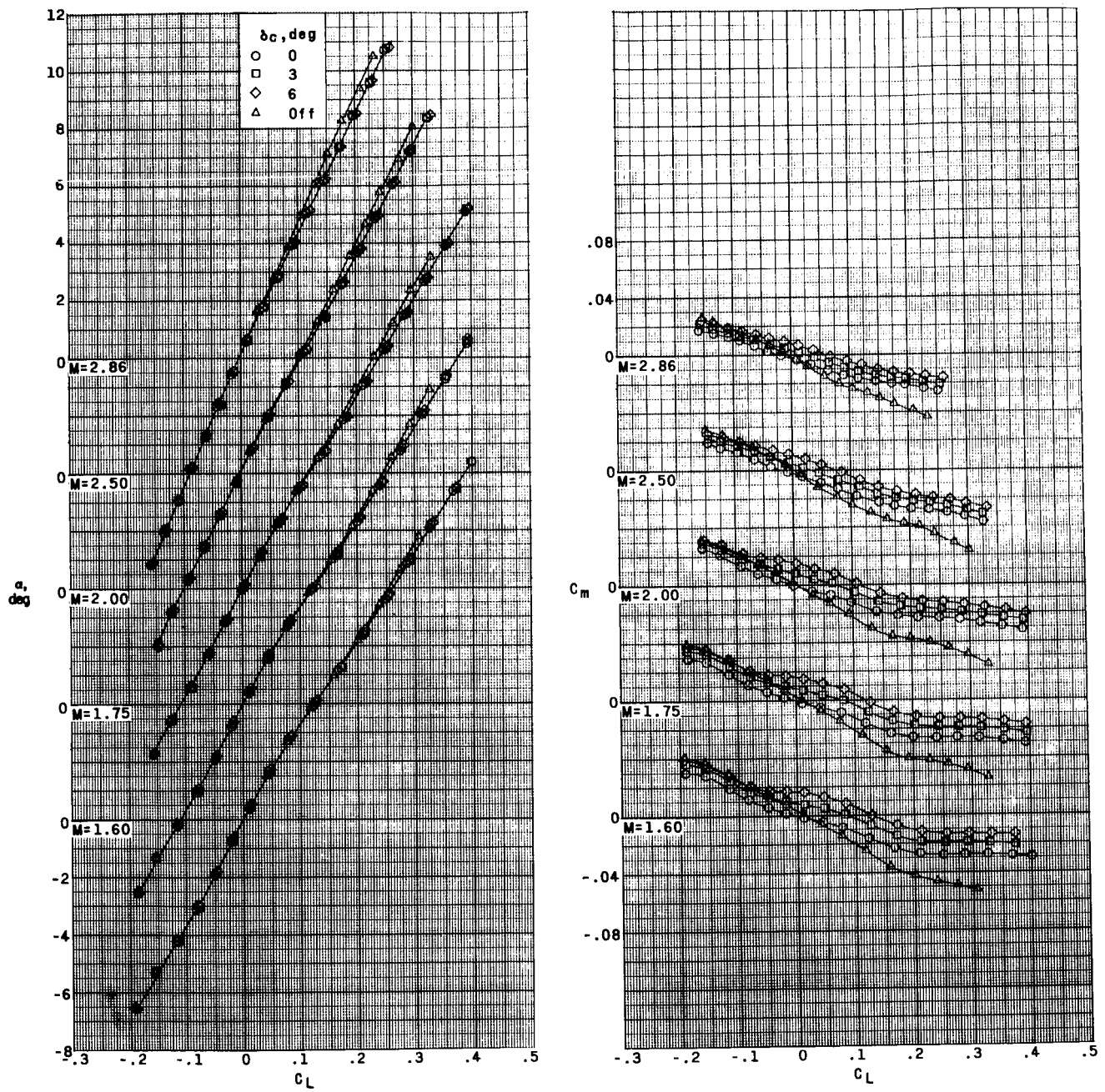

(a) Variation of α and C_m with C_L.

Figure 9.- Effect of canard on aerodynamic characteristics in pitch. Simulator on; $\Lambda = 75^\circ$; $\Lambda_{FW} = 79.75^\circ$; $\delta_h = -0.26^\circ$ (low position); vertical tail on.

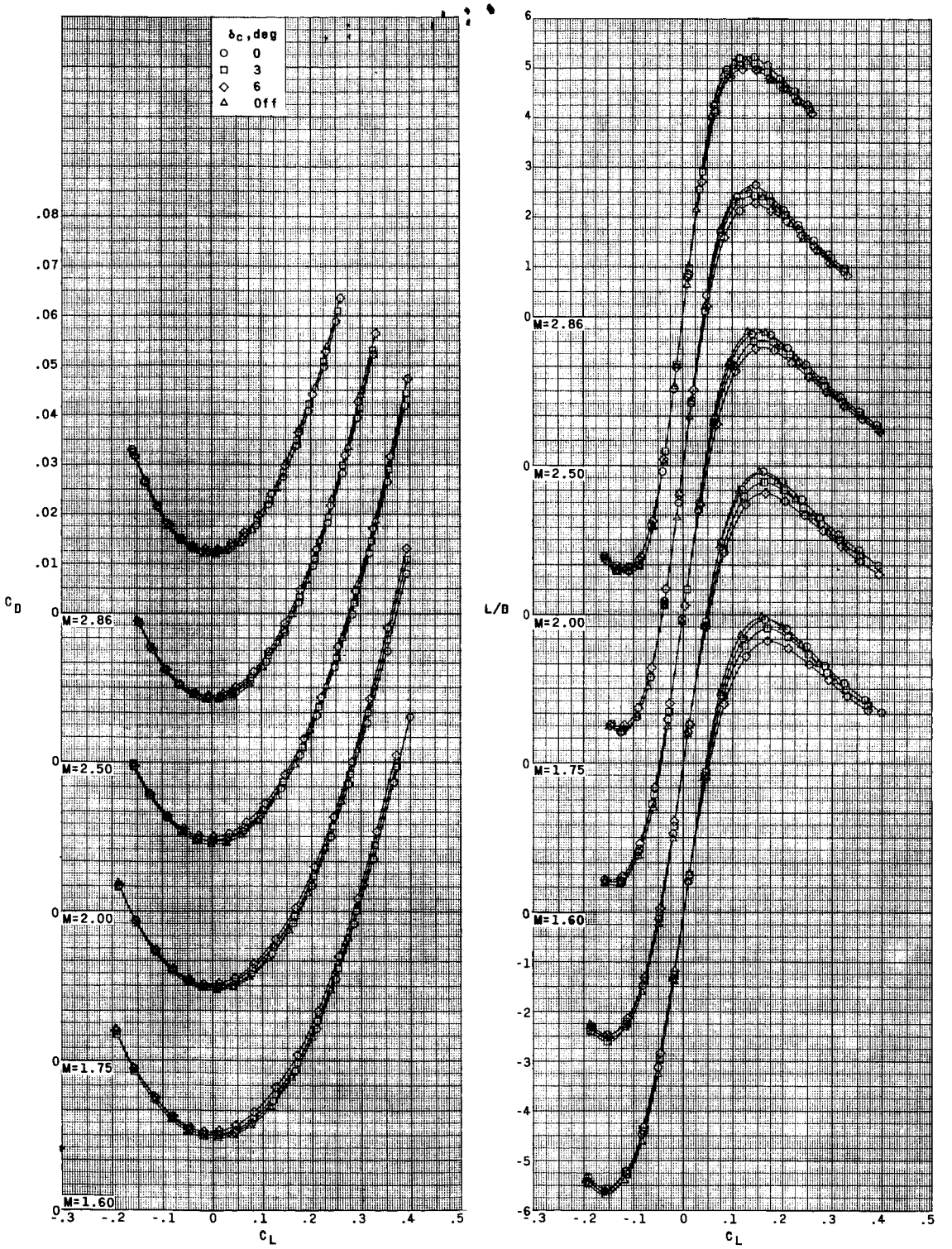

(b) Variation of C_D and L/D with C_L.

Figure 9.- Concluded.

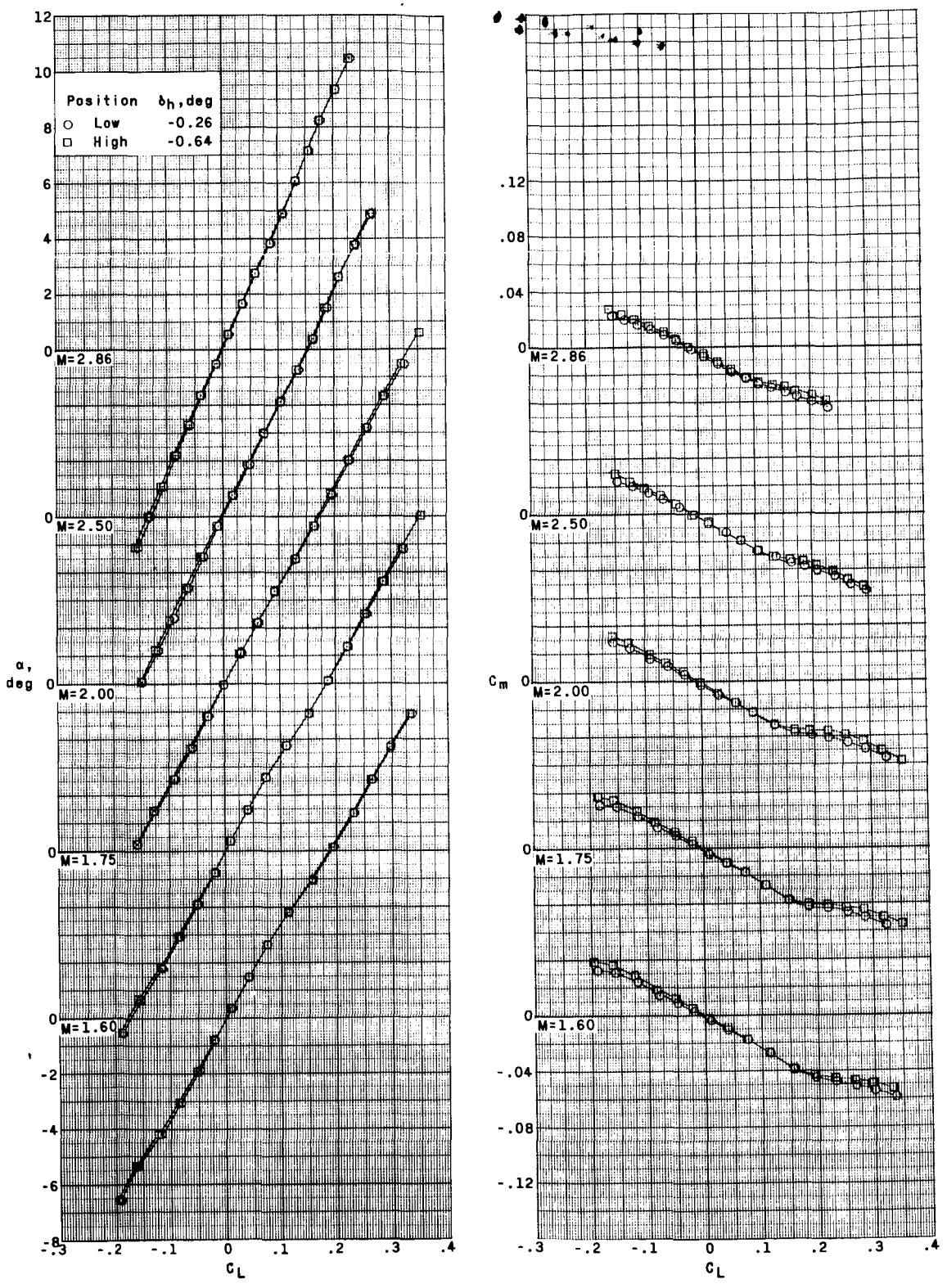

Figure 10.- Effect of horizontal-tail position on aerodynamic characteristics. Simulator off; no engines; $\Lambda = 75^{\circ}$; $\Lambda_{FW} = 79.75^{\circ}$; vertical tail on; δ_c = off.

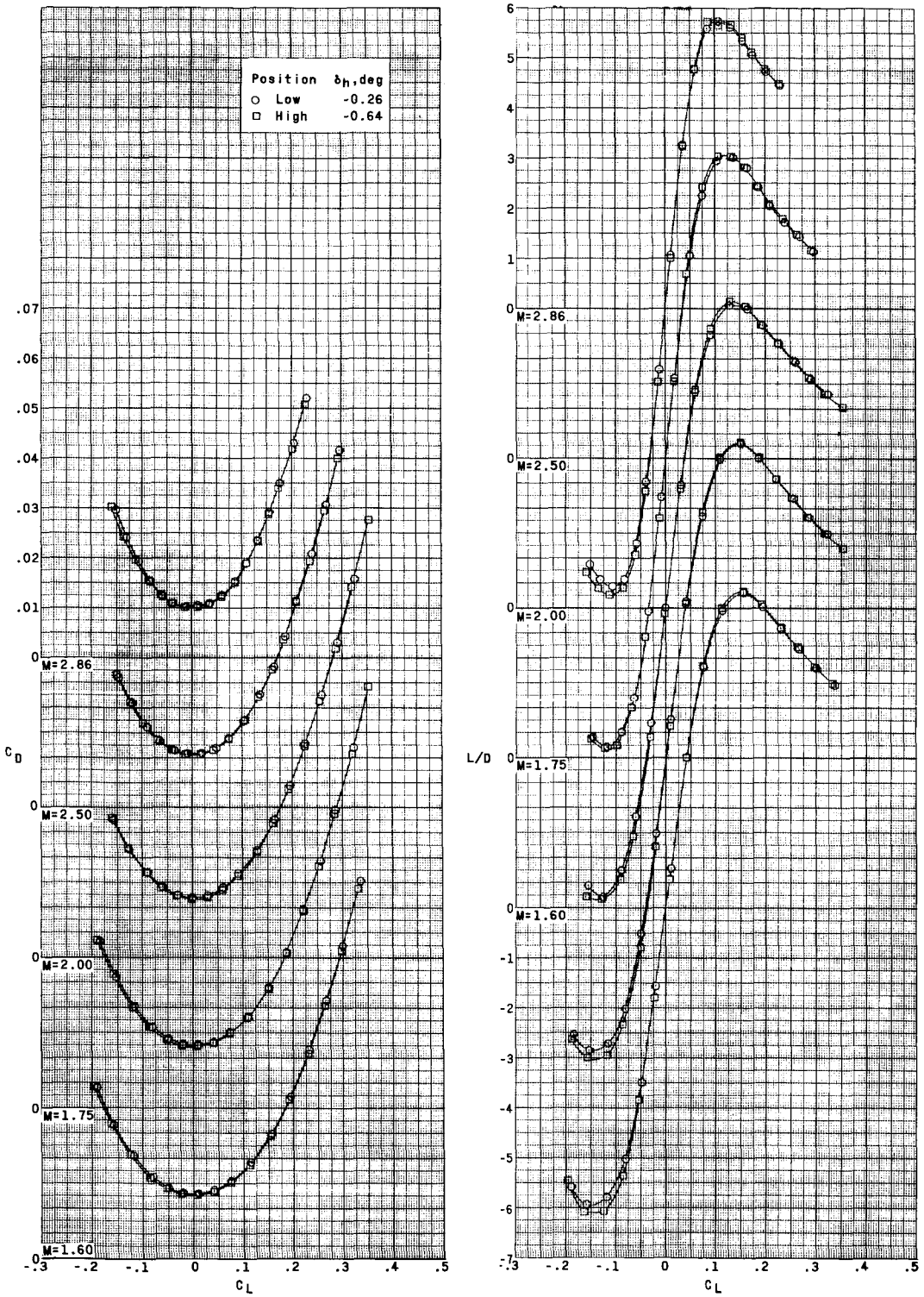

(b) Variation of C_D and L/D with C_L.

Figure 10.- Concluded.

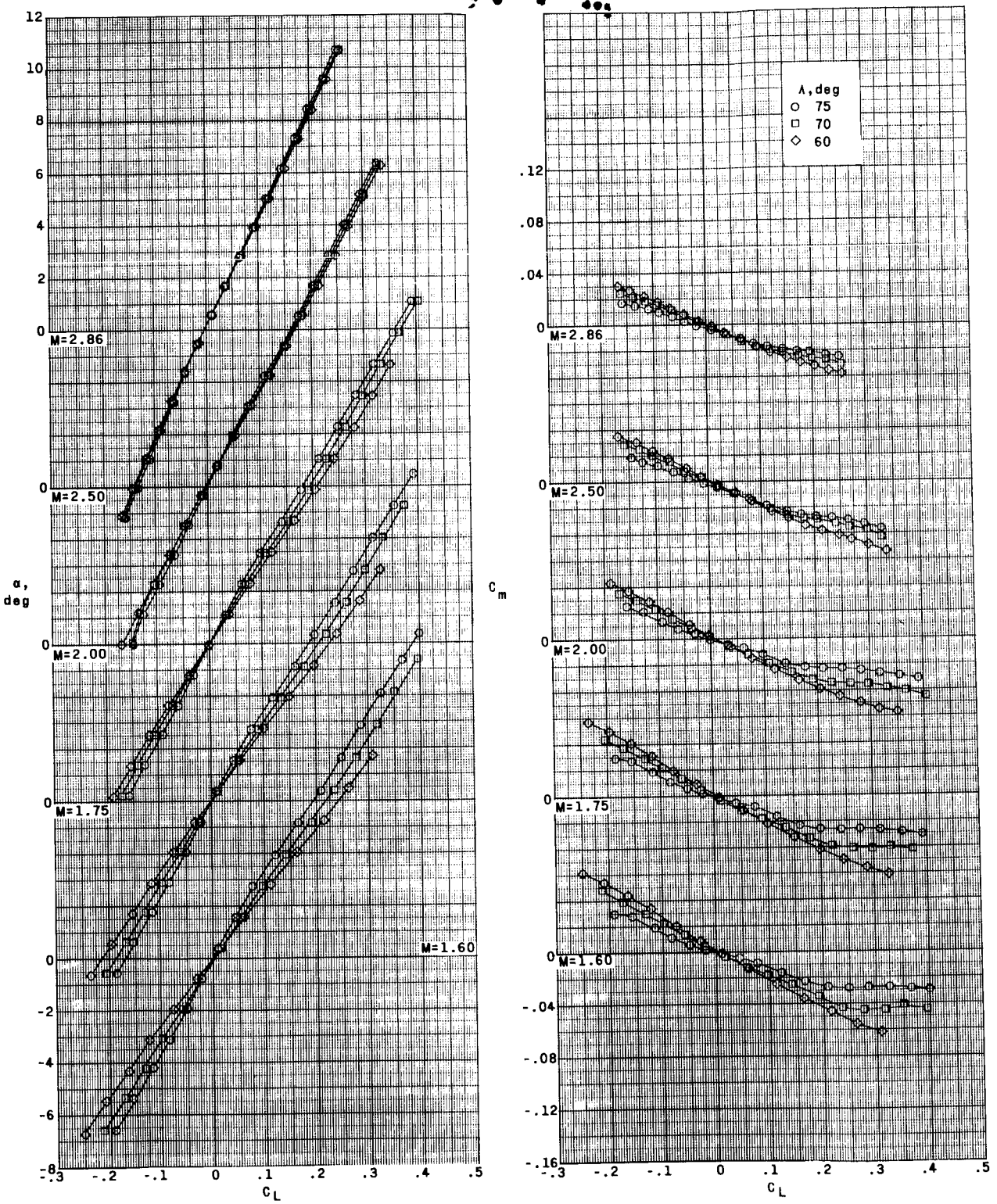

(a) Variation of α and C_m with C_L.

Figure 11.- Effect of wing sweep on aerodynamic characteristics in pitch. Simulator on; $\delta_h = -0.26^\circ$ (low position); vertical tail on; $\delta_c = 0^\circ$.

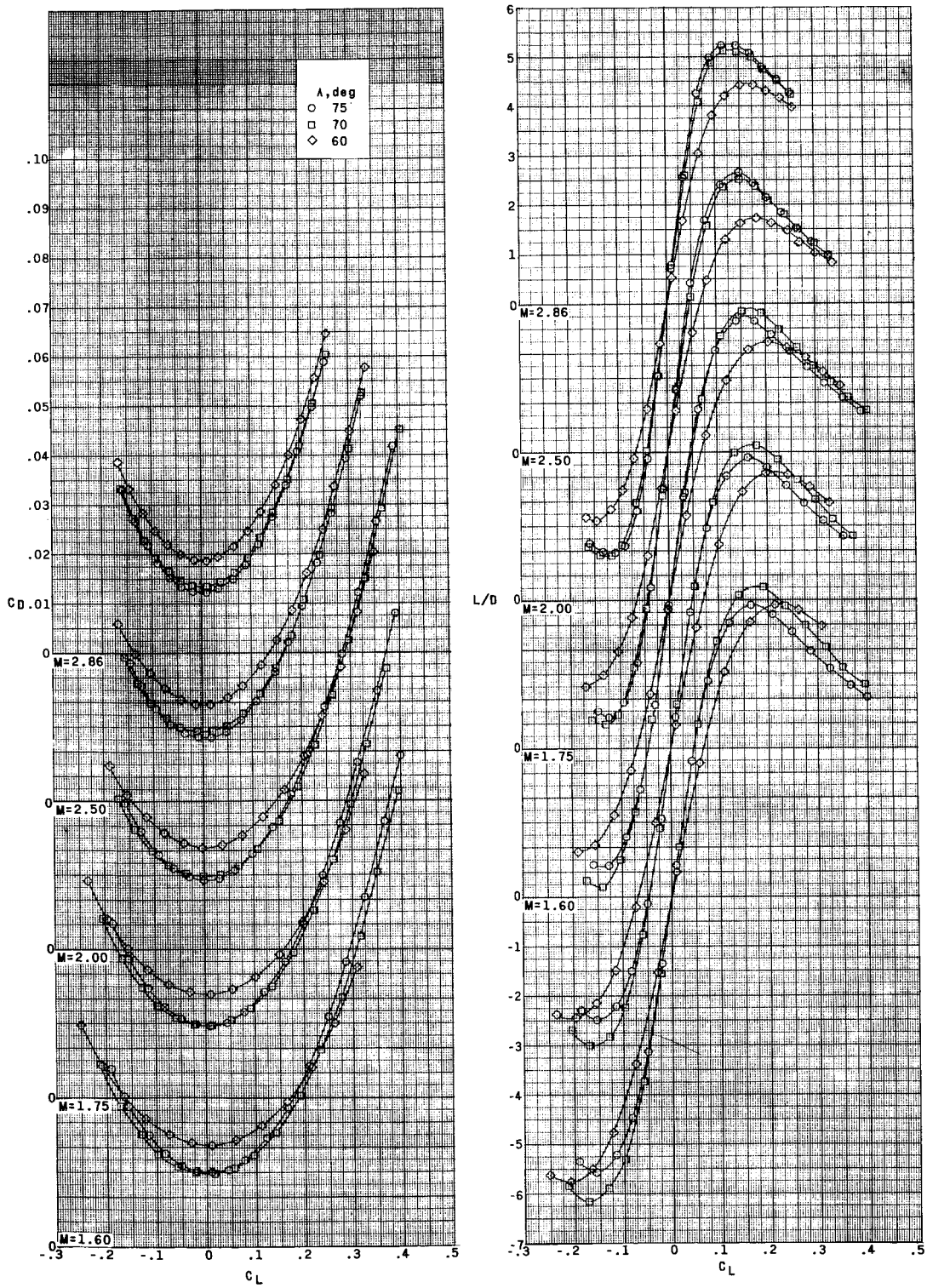

(b) Variation of C_D and L/D with C_L.

Figure 11.- Concluded.

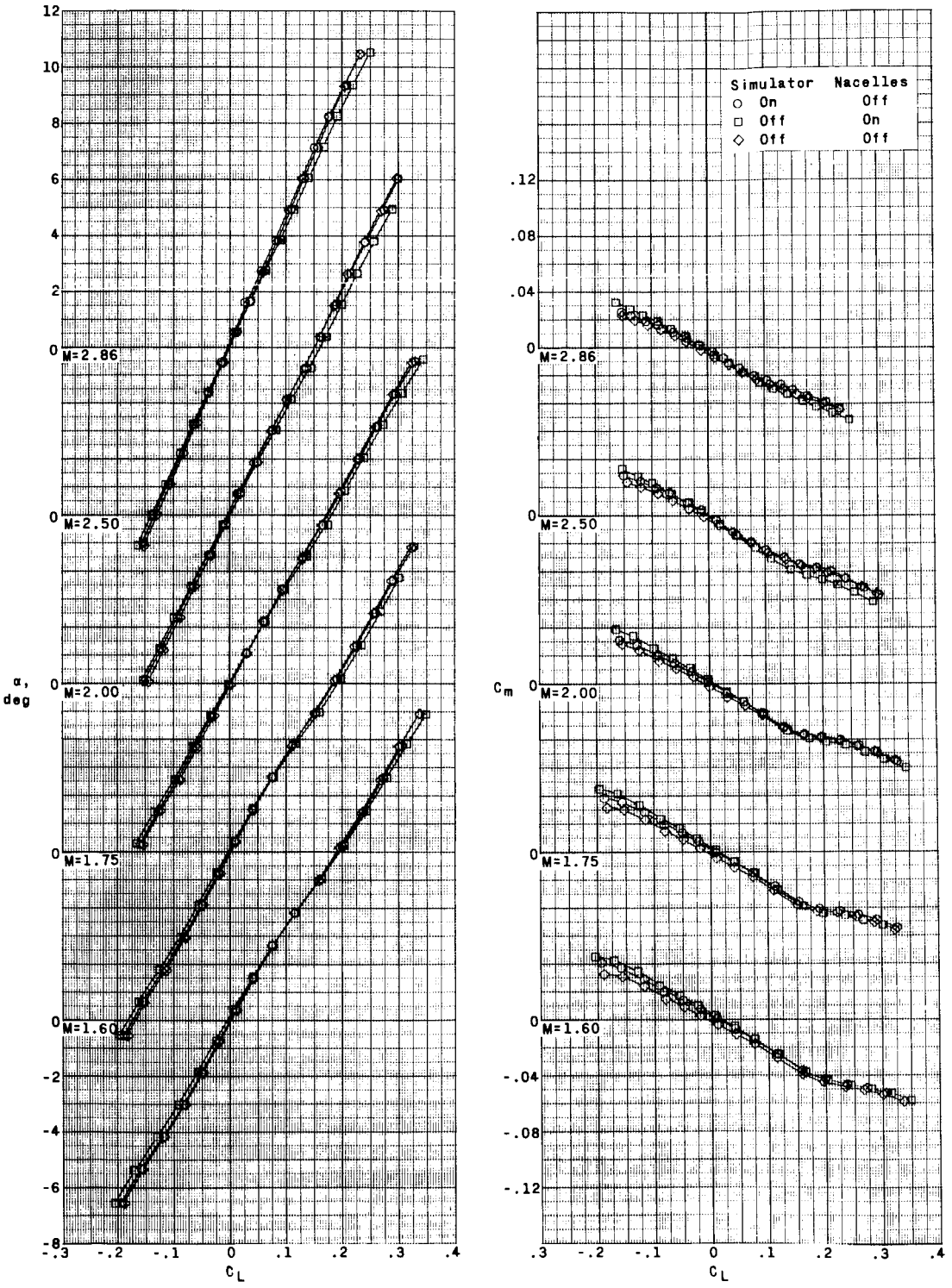

(a) Variation of α and C_m with C_L.

Figure 12.- Effect of engines on aerodynamic characteristics. $\Lambda = 75^\circ$; $\Lambda_{FW} = 79.75^\circ$; vertical tail on; $\delta_h = -0.26^\circ$ (low position); δ_c = off.

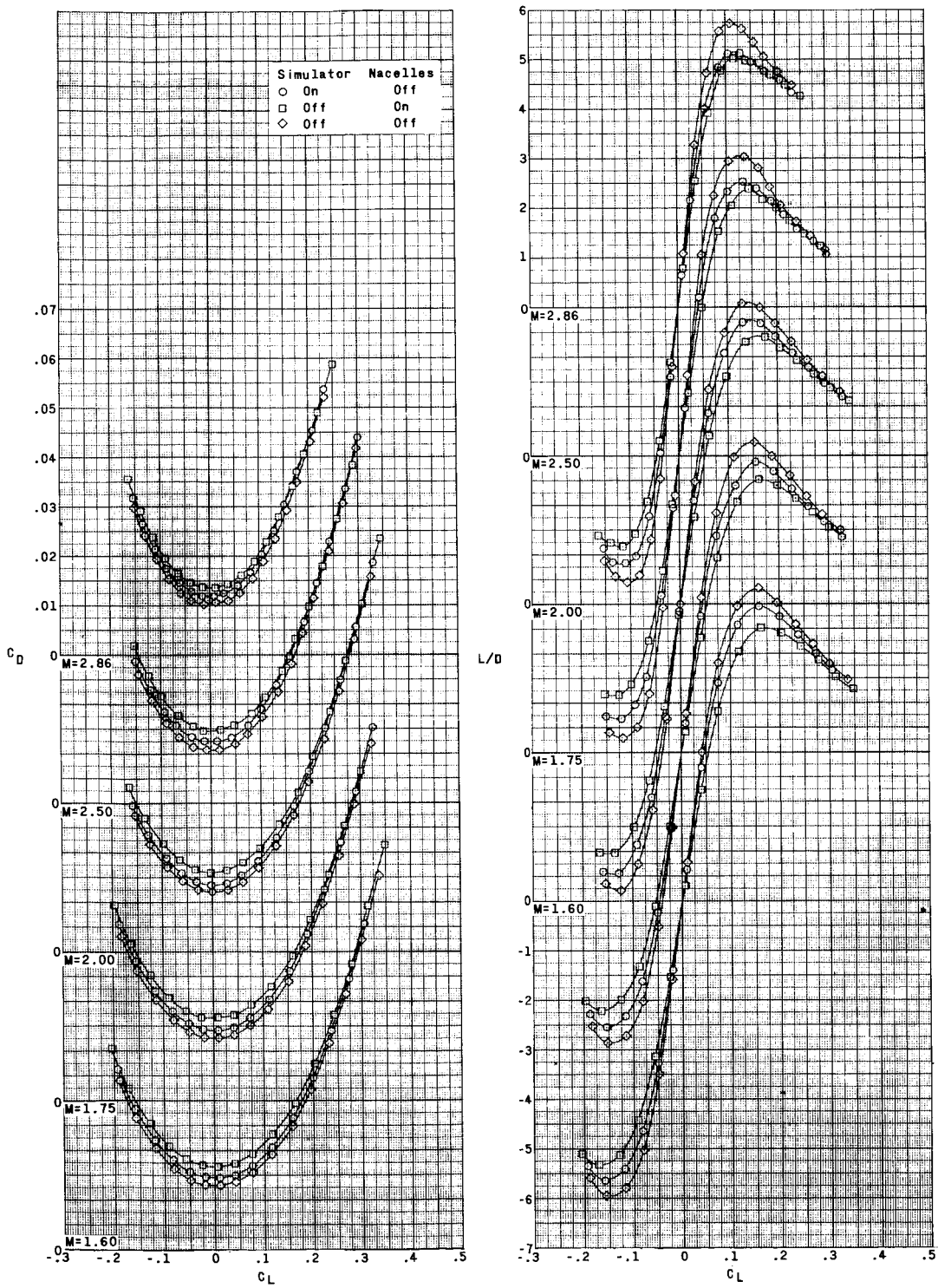

(b) Variation of C_D and L/D with C_L.

Figure 12.- Concluded.

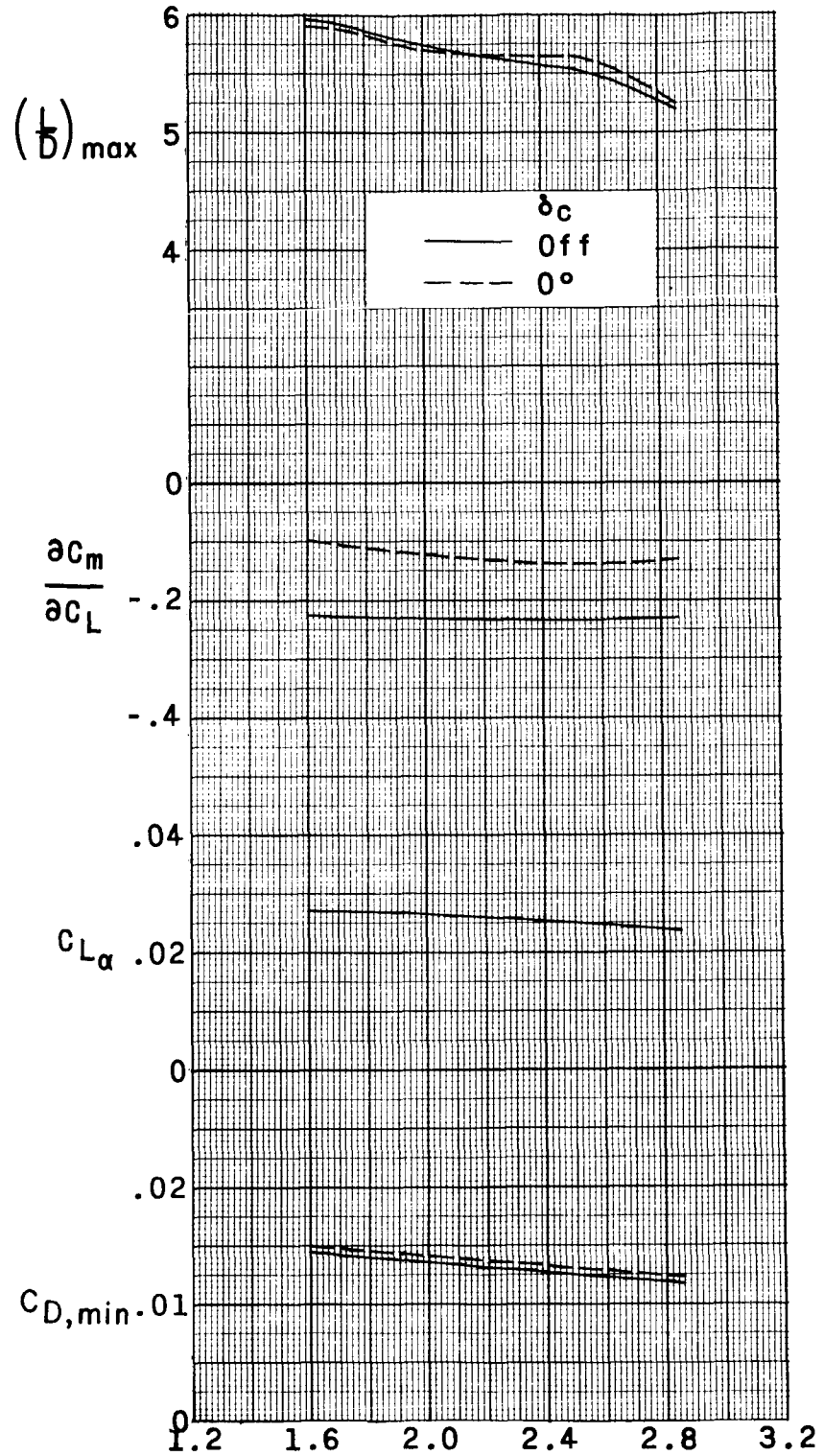

Figure 13.- Summary of longitudinal characteristics in pitch of the basic configuration both with and without the canard. Simulator on; $\Lambda = 75^\circ$; $\Lambda_{FW} = 79.75^\circ$; vertical tail on; $\delta_h = -0.26^\circ$ (low position).

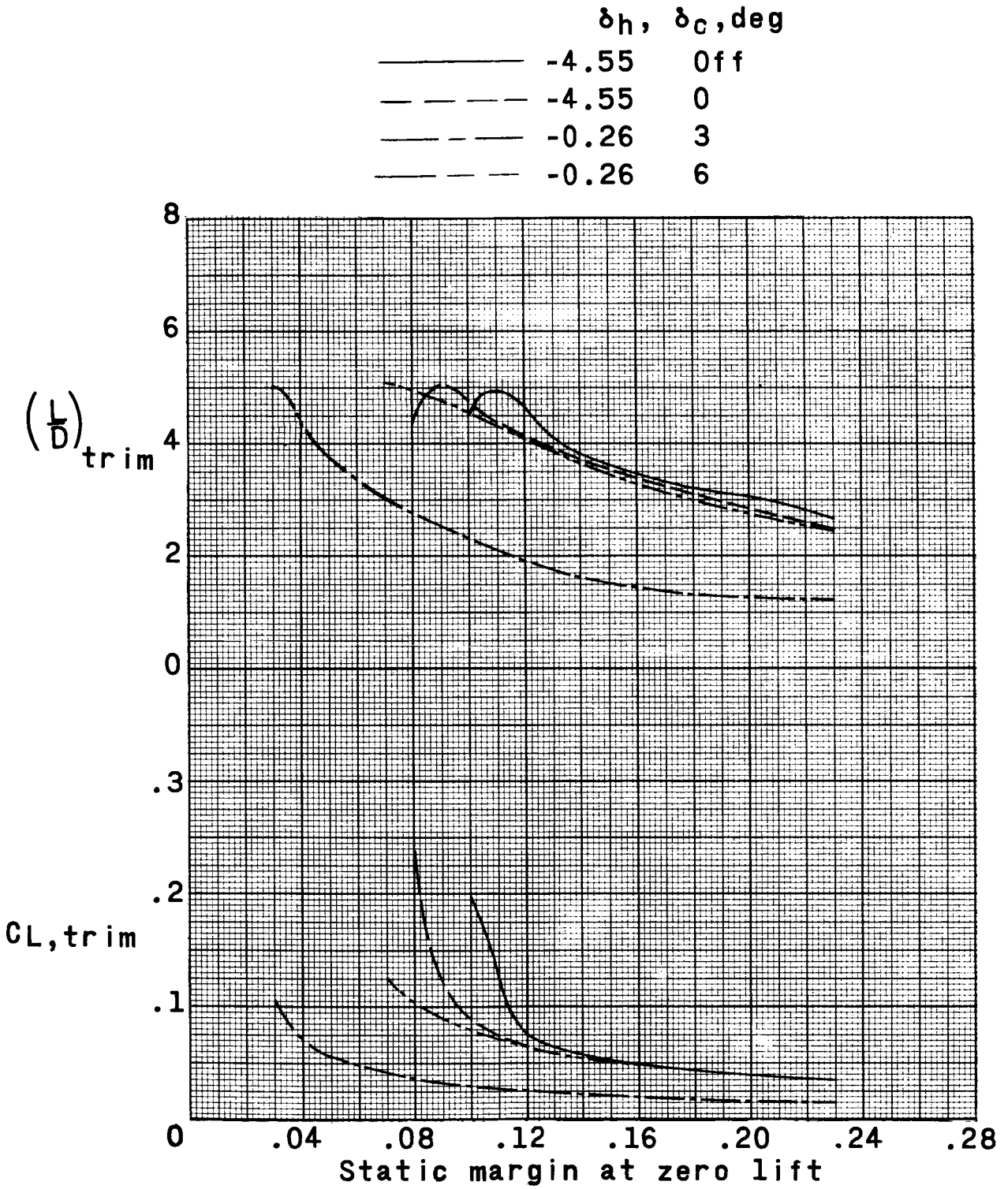

Figure 14.- Effect of change in static margin on $C_{L,trim}$ and $(L/D)_{trim}$ at $M = 2.86$. Simulator on; $\Lambda = 75^{\circ}$; $\Lambda_{FW} = 79.75^{\circ}$; vertical tail on; δ_h at low position.

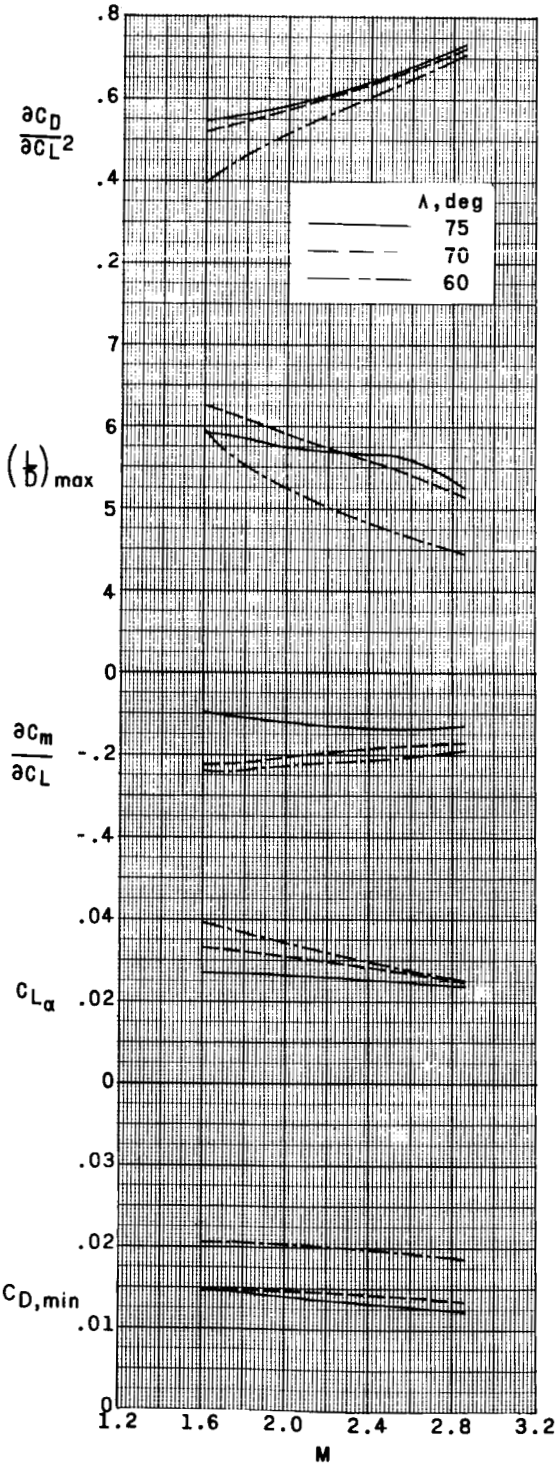

Figure 15.- Summary of effects of Λ. Simulator on; vertical tail on; $\delta_h = -0.26^\circ$ (low position); $\delta_c = 0^\circ$.